CHAPTER (4)

RESULTS AND DISCUSSION

CHAPTER (4)

RESULTS AND DISCUSSION

4.1. Preparation and Characterization of High Coercivity Barium Ferrite Powder

4.1.1. Introduction

Hexagonal barium ferrite ($BaFe_{12}O_{19}$) phase was prepared by the co-precipitation method as mentioned before in chapters 2 and 3

After all these strenuous effort from the scientists to produce high quality barium ferrite phase avoiding the undesirable characteristics. Some defect still not recovered yet as, why always little success accompany the ultra fine powders, the effect of NaCl not recover yet, particle size distribution and final Fe/Ba molar ratio in the precursor.

For these reasons and for more precisely, it is necessary to study essentially the nine preparation parameters mentioned before besides the new parameters in detail during the synthesizing of the powder. Also the good selecting from first for the preparation conditions is important to get in the final magnetic material with desirable characteristics and to avoid the undesirable one.

4.1.2. Conditions for Formation High Coercivity Hexagonal Barium Ferrite Powder.

(i) *Ferric/Barium molar ratio (n):*

The common starting materials for preparing barium ferrite by co-precipitation methods are barium nitrate and iron nitrate [10,11,31,32] or barium chloride and ferric chloride [8,9,19-21,23,24]. The last one is preponderant and always exhibits good magnetic properties than the other one. Barium ferrite can be formed according to Fe/Ba ratio $6 \leq n \leq 14$. The best magnetic properties were obtained when n was taken between 10.6~12. (Haneda and Morrish[20], maximum H_c at n=11). W.Ross [11] , recorded the high value at n=11.6. Pure Iron chloride $FeCl_3.6H_2O$ and pure barium chloride $BaCl_2.2H_2O$ (Wako Japan) were used in the present study as raw materials. The molar ratio n = Fe/Ba was checked prior to the preparation of the powder in the range 11~12. n=11 was selected as a starting molar ratio.

(ii) *PH value of solution:*

(Hydrogen number): in the previous works, authors [8-10] prepared hexagonal barium ferrite in the pH range 10~13, where the selection of PH values depends on the other preparation conditions. The higher pH values are favored for the suitability of medium for barium ferrite precipitation. On the other hand the high PH value leaves behind it an excess of NaCl in the precursor, which affects the magnetic characteristics of the obtained powders. So the intermediate value of PH 11~12 is desirable. In the present study we have used pH=12, prepared by adding 40 g NaOH and 11g Na_2CO_3 to 400ml distilled water.

During the reaction pH, value was tested and kept constant by using HCl and Na_2CO_3 solution.

(iii) *The sequence of reagent addition:*

The sequence means adding barium chloride and ferric chloride solution to sodium hydroxide and sodium carbonate solution or vice versa. This new scope appeared only in the first of 2002, during the present study. Our results agreed with Janasi et al.[23].The best results for the coercivity was obtained by adding $NaOH/Na_2CO_3$ solution to $BaCl_2/FeCl_3$ solution with vigorous stirring . This is owing to the nature of precursors that depends strongly on the precipitation circumstances during chemical reaction.

(iiii) *The presence of NaCl:*

The presence of NaCl during barium ferrite formation reaction has a negative effect on the magnetic properties (it lowers both of coercivity and magnetization). This was studied by Sakai et al. [24] and recently Janasi et al. [23], also studied X-ray scattering for washed and unwashed precipitates of the reaction of BaCl and $FeCl_3$,but the effect of NaCl on the reaction temperature is not covered yet. In the present study the effect of precursor washing on the presence of residual NaCl and its reflection on the product quality was carried out by using differential thermal analysis (DAT) and magnetic measurements. The obtained powder divided into four groups *unwashed, single washed, double washed, and triple washing times* by hot distilled water. Figure (4.1) illustrates DTA for the mentioned samples. Endothermic peaks appear at around 100°C refer to the water vaporization and the second sharp endothermic peaks around 635 ~ 900 °C is due to the melting of NaCl which increase by decreasing the

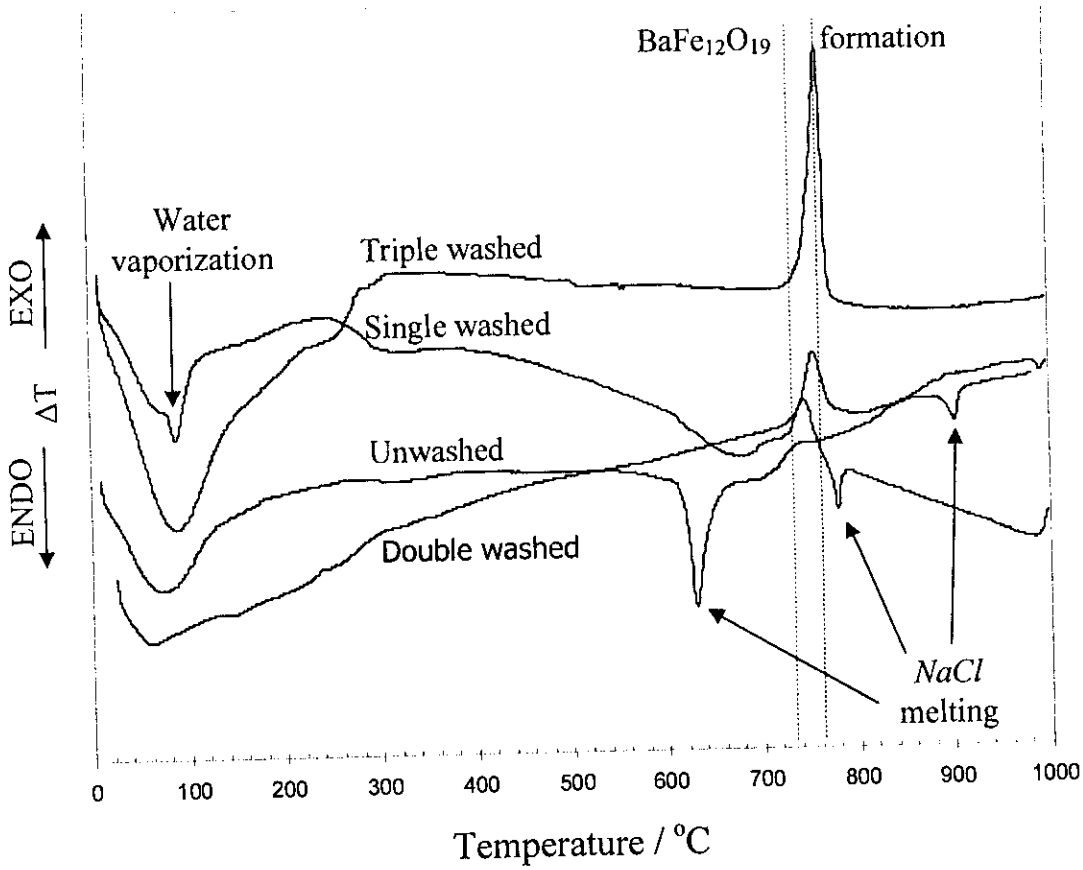

Fig (4.1). *Differential thermal analysis for unwashed, single, double, and triple washing barium ferrite precursors.*

amount of residual NaCl in the precursor with further washing. In the case of unwashed precursor, barium ferrite formation peak vanished . At single time washing NaCl melting temperature peak was reduced and shifted to higher temperature 780 ^{o}C. A broad exothermic peak around 750 ^{o}C emerged due the formation of barium ferrite, as reported previously ,barium ferrite M phase starts formation at 700 ^{o}C, and nearly single phase materials can be obtained after annealing at 900 ^{o}C, or above [76]. For the three times washing precursor, NaCl melting peak disappeared while barium ferrite crystallization peak became more sharp and shifted to higher temperature 765 ^{o}C .The presence of NaCl acts as a catalyst and shifted the crystallization temperature of barium ferrite down .

(v)- *Grinding level:*

Particle size is an important factor control the coercivity H_c of the powder. In general, when H_c is initially low, milling of the particles leads to an increase of its value up to a certain particle size (within domain size 0.1 ~0.5μm). Contradictory , when H_c is initially high (in the range of domain size) , milling will reduce particle size to lower values much smaller than domain size leading to a reduction in H_c [26]. The particle size varies by milling from multidomain (several microns) to single domain (0.1~0.5μm) to superparamagnetic domain (0.02> μm) [14,19,20,77]. Therefore coprecipitation method prevents grain growth ,and particles are free from the stresses and strains caused by particle diminution in milling ,so high coercive force can be expected. It is also concluded that lattice defects rather than superparamagnetic fine particles introduced by milling greatly affect the intrinsic coercive force of barium ferrite powders [26].

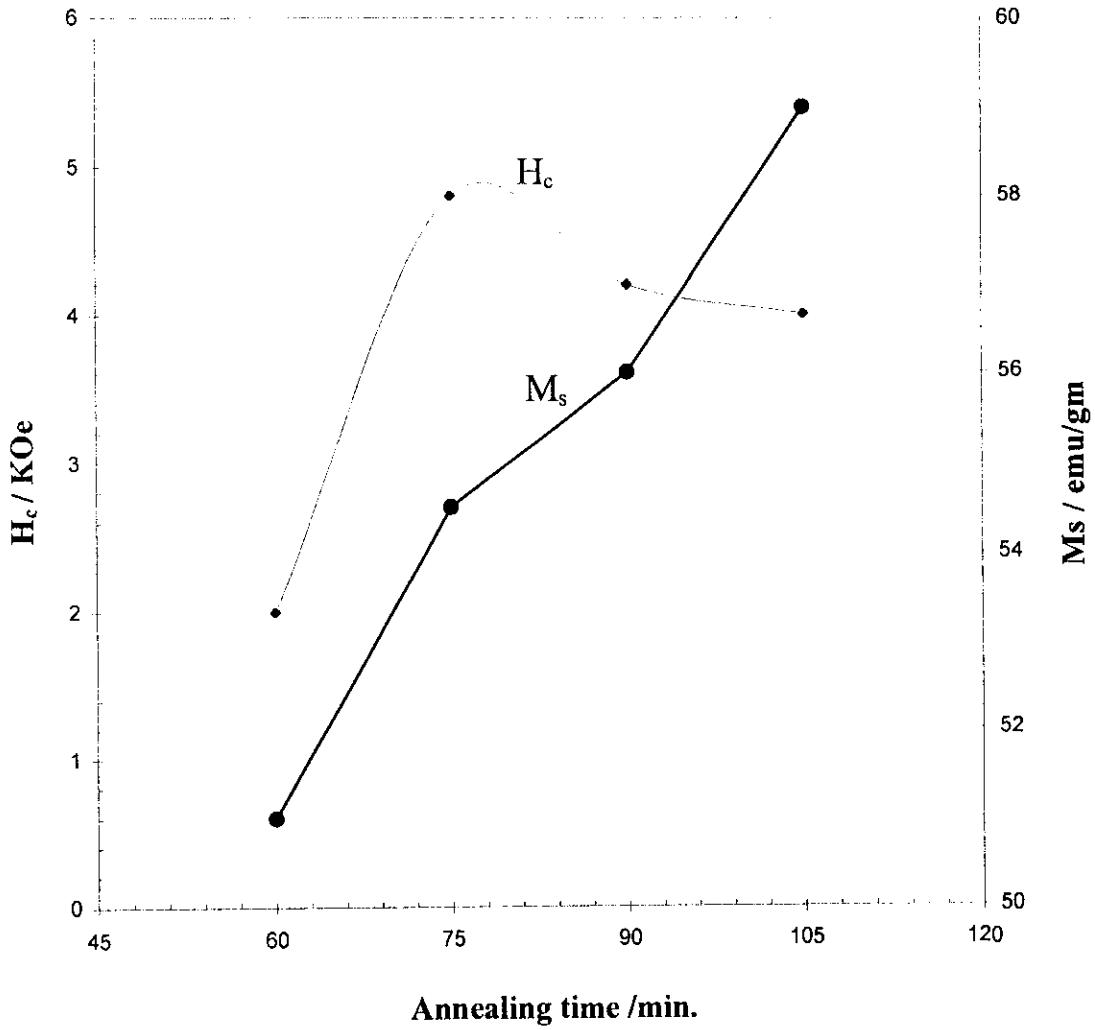

Fig (4.2). *The variation of saturation magnetization (M_s) and coercive force (H_c) for rough powder with increasing annealing time at 925 °C.*

The ferrite samples used in the present study prepared by two grinding methods. After the precursor was dried in tube furnace at 100 °C for. Firstly the powder was mechanically milled to reduce the particle size near to the domain size before annealing at the desired temperatures, after heat treatment the ferrite was grind again manually (little hand grinding in mortar) to reduce particles aggregation ,then the sample was heated for short time to remove lattice defects caused by grinding . The process of little grinding/ heat treatment was repeated three times until the magnetic properties of ferrite reached its highest level as shown in Figure (4.3). H_c increases by improving the powder dispersibility, reducing particle size and treating the lattice defects, where a little decrease in saturation magnetization was recorded by developing this process. . This enables us to synthesis successfully high coercivity barium ferrite power having small particle size.

In fact we failed in further attempts to exploit this way to prepare powder with similar characteristics or to use it for getting large amounts from the powder. This is due to as mentioned before, little successes always accompany the fine powders, and the true reasons for that will be discusses later.

From the above discussion it was definite to give our attention to the dispersibility and particle size distribution. These two factors were not studied before and at the same time they have a perceivable effect on the magnetic properties of ferrite [78].

(iv)- *Treatment temperature:*

The effect of temperature on the coercive force and saturation magnetization was firstly studied [8,19-20], the results indicated that, the increase of particles

(iiiv)- *Atmosphere oxygen or air:*

Atmosphere may be oxygen or normal atmosphere (air) , by using oxygen it is possible to decrease the temperature and annealing time, where the reaction happens more quickly than the normal one .

(ix)-*Addition of protective agent:*

Where saturation magnetization and coercive force depend strongly on the particle size, morphology, and microstructure of the materials. Therefore it is interesting and important to control size, shape, and chemical homogeneity. The addition of protective agent, such as water soluble polymer during precipitation, or (NaF) during milling, may be a promising method to overcome some of these problems [24,25,28].

(x)- *Particle size distribution:*

Superparamagnetic particles generate by milling and annihilate by annealing. On the other side, the side effect for the temperature is to increase the grain size for the large particles than the desired range. Then the particle size distribution after heat treatment will be similar before heat treatment. So it will be useful to classify the particle size distribution to narrow size distribution and treat every one according to the appropriate conditions. Fine powder is not necessary for this work, where the aim of this work is to prepare a rubber-ferrite magnet(non recording materials) .So the powder could be classified in the range 45~200μm which is large comparing to the particle size .

(xi)- *Fe/Ba molar ratio in precursor:*

Since Barium hydroxide and ferric hydroxide have different solubility in water (Barium hydroxide is slightly soluble i.e. solubility product at 25 °C = $10^{-3.6}$[28]

and the optimum reaction temperatures are function of molar ratio n [79]. The Fe/Ba molar ratio (n) was initially examined in the precursor by EPMA. The aim of testing n in the precursor not in the solution or after washing is to study the effect of grinding also on the molar ratio, so n was examined just before heat treatment and after all the prior procedures were finished. The experiment was done on the multi size high coercivity powder and the results will be discussed later.

4.2. Preparation of Hexagonal Barium Ferrite

4.2.1 Fine powder:

In the present work hexagonal barium ferrite in the form of fine powder was prepared by grinding the rough powder after precipitation using a grinding machine, before considering the study of the effect of preparation conditions of prepared powder. Figure (4.3) a and b illustrates the size and hysteresis loop of heat treatment powder at 925 °C for 1.5 hours. It is clear that the particles aggregate indicating their lower size, where B-H curve shows a kink in demagnetization direction which reflects the effect of particle surface interaction and the presentce of different undesirable phases. On the other hand, the apparent low coercive force (4.6 KOe) in the milled state could be attributed to the reverse domain nucleation at sites of imperfection caused by milling.

The mentioned powder, which is represented in figure (4.3), is retreated again by soft hand grinding and heat treatment for a bout 10 min to minimize the effect of imperfections caused by milling. After that, the particle were examined by high magnification TEM to clarify the effect of milling on the particles in the

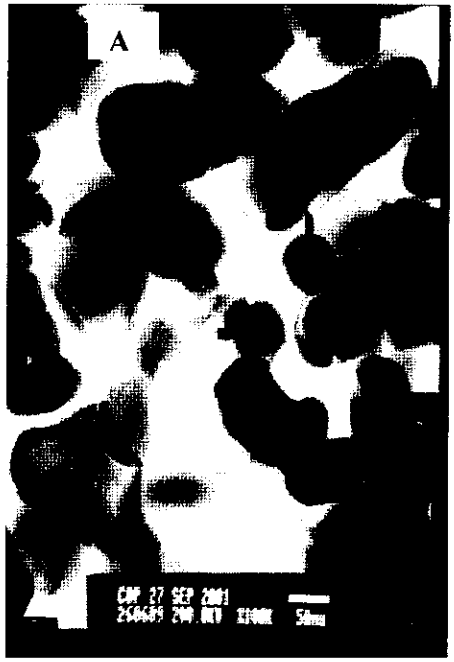

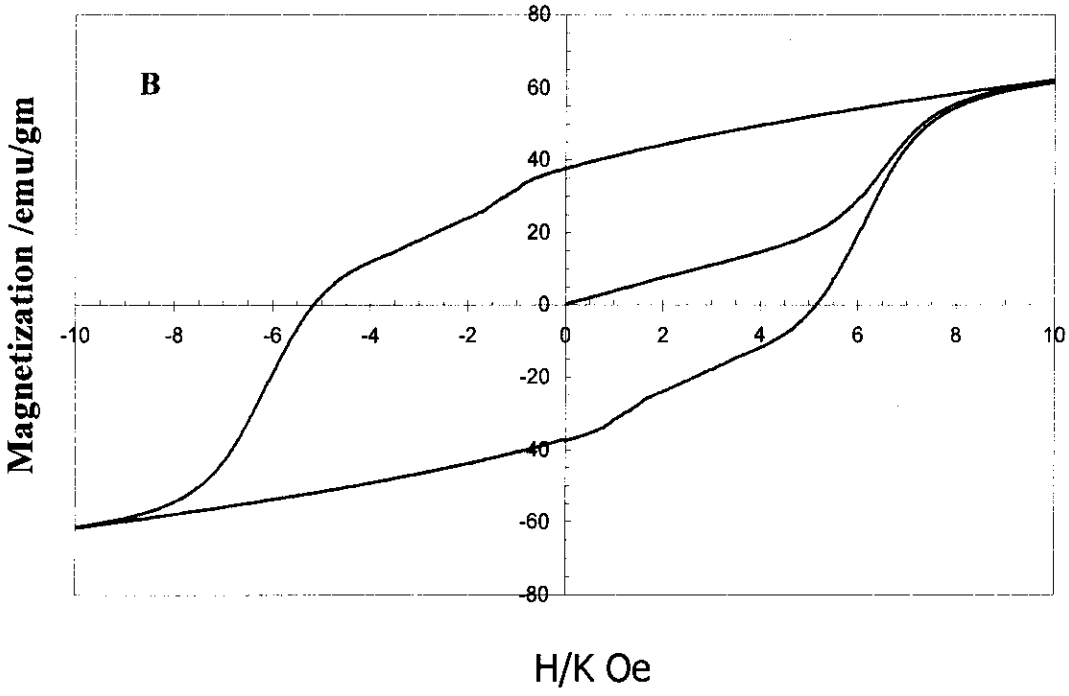

Fig. (4.4). *A TEM photograph and B Hysteresis curve of the powder illustrated in figure (4.3) after retreatment .*

magnetic form figure (4.4a). It clearly illustrates that the particles are disaggregated in comparison with the previous case. In addition no significant change in the particle size was recorded but some of the particles are broken under milling .The magnetic behavior became more regular as a result of powder disaggregating besides the reduction of the number of inverse domain . This leads to the improvement of saturation magnetization and coercive force at the same time figure (4.4b).

The powder was retreated once more as the mentioned procedure , the examination illustrates homogeneity and dispersibility of the powder therefore the , demagnetization curve became more smooth due to the reduction in the surface energy among the ferrite particles and the numbers of inverse domain leading to an increase in H_c to 5.42 KOe . A little reduction in the particle size was recorded due to the increase of the number of fine particles as a result of the twice milling, this causes a reduction in the saturation magnetization from 62 to 59 emu/g. figure (4.5) a and b illustrates the microstructure and hysteresis loop respectively.

Coercive force, saturation magnetization at 10 K Oe and particle size for the three mentioned powders are listed in table (4.1) for comparison to illustrate improvement of ferrite powder under successive grinding and heat treatment process .The final obtained powder recorded a reasonable coercive force (5.42 K Oe) with low saturation magnetization (59 emu/g).

After achieving the mentioned results, it was noticed that, the higher coercive force and magnetization could be obtained only by using small layer or a little amount from the powder during heat treatment. Whereas by increasing the

powder thickness or large amount in the furnace, coercivity decreases sharply ,in addition to the inhomogeneity in the magnetic behavior.

This abnormal behavior in the magnetic properties of $BaFe_{12}O_{19}$ with increasing the powder amount in the furnace during heat treatment may be resulted from the oxygen deficient inside the powder. This phenomenon was studied as follows;

The powder used in figure (4.3) was repeated in a large amount from the same powder to illustrate the effect of air or (oxygen) on the coercive force and magnetization of obtained powder .The recorded hystersis loop for the powder is shown in figure (4.6). It illustrates a reduction of both coercivity and magnetization from 4.65 KOe and 56 emu/g to 1.9 KOe and 51 emu/g respectively combined with changing in the demagnetization curve as an evidence of unhomogeneity in the ferrite phase.

Another attempt was done for the double grinding and heat treatment of the powder with large amount of such powder. Hystersis loop is given in figure (4.7). One notices that, the probability of synthesizing high coercivity barium ferrite powder from fine powders is still difficult. In figures (4.6) and (4.7), saturation magnetization (in case of using large amount of powder) tend to decay sharply at low negative magnetic field comparing with higher values (in the case of small layer of powder figures (4.3) and (4.4)) .The decrease of magnetization and coercive force for the present powder is a strong evidence for the presence of the other phases work as a magnetization inhibitor for hexagonal barium ferrite phases , they lead to the inhomogeneity of the powder reaction together with oxygen distribution during heat treatment .

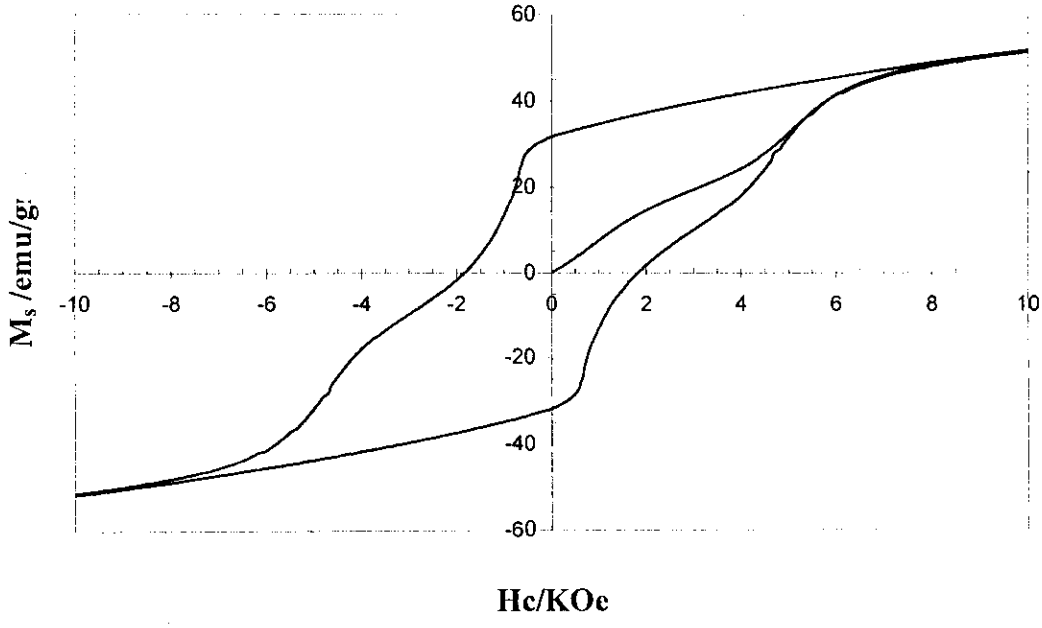

Fig (4.6). Hysteresis *curve of the powder represented in figure (4.3) after re-annealed by a large amount.*

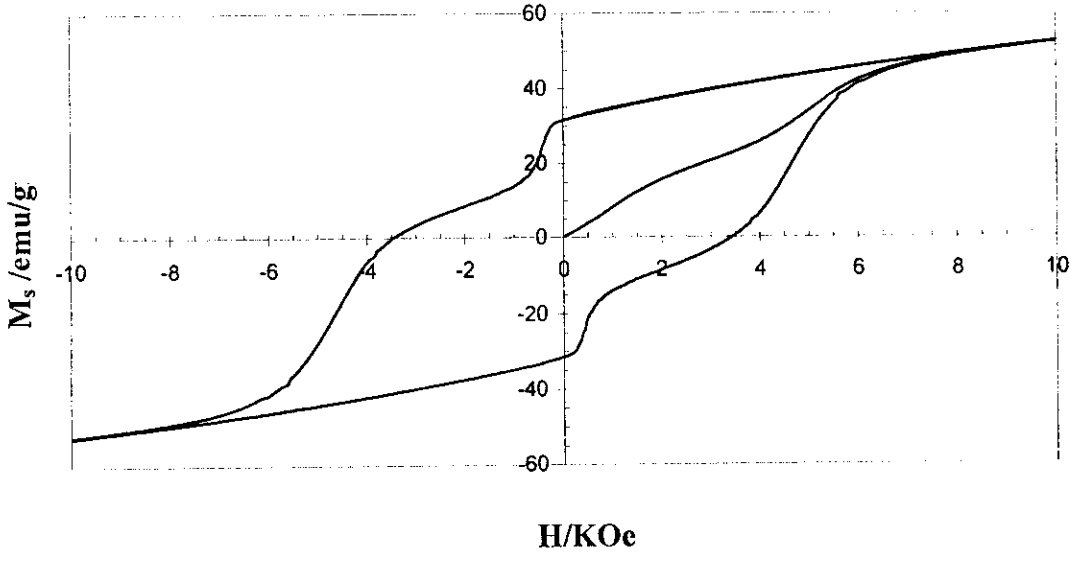

Fig (4.7) *Hysteresis curve of the powder represented in figure (4.5) after re-annealed by a large amount.*

Process	H_c (K Oe)	M_s (emu/g)	D (nm)
0	4.65	56	150~100
1	5.25	62	~100
2	5.42	59	~100

Table (4.1) The *variation of coercive force , saturation magnetization ,and particle size with the development of grinding/ annealing processes*

Powder	Size distribution (μm)
1	Rough powder
2	After elimination of powders less than 45 μm from the rough
3	Higher than 200
4	200~100
5	100~75
6	Less than 45

Table (4.2) Classification *of the powders according to the particle size and size distribution.*

Also, it is noticed that the exterior surface of the powder, which exposed for an excess of air in the furnace during heat treatment , was more darkly brown than the interior one owing to the different phases and concentration of ferrite, this is a function of the powder color [43]. Figure (4.8) shows the photograph of both the exterior and interior layers of the powder, which is illustrated in figure (4.6) after heat treatment.

The study of reaction was extended in the absence of air current for the powder illustrated in figure (4.5) and the obtained hystersis loop is illustrated in figure (4.9). The decay in demagnetization behavior becomes more drastic leading to low coercive force. This effect is due to the change in the oxygen fraction in the furnace leading to different phases. H.J. Van Hook [7,60] has pointed out that barium ferrite phases changed by oxygen deficient and oxygen pressure during the chemical reaction.

Figure (4.10) illustrates X-ray diffraction pattern for sample treated in figure (4.9). Different peaks appeared related to different ferrite phases are recorded. The presence of these phases may be the reason for affecting the magnetic properties in the case of fine powder as a result of deficient of oxygen distribution inside the powder .This controls the reaction which leads to a multi-phase powder.

4-2.2 Size distribution powder

In this section barium ferrite with different particle size and narrow size distribution was prepared in air current during heat treatment to avoid the effect of oxygen deficient and the effect of fine powders.

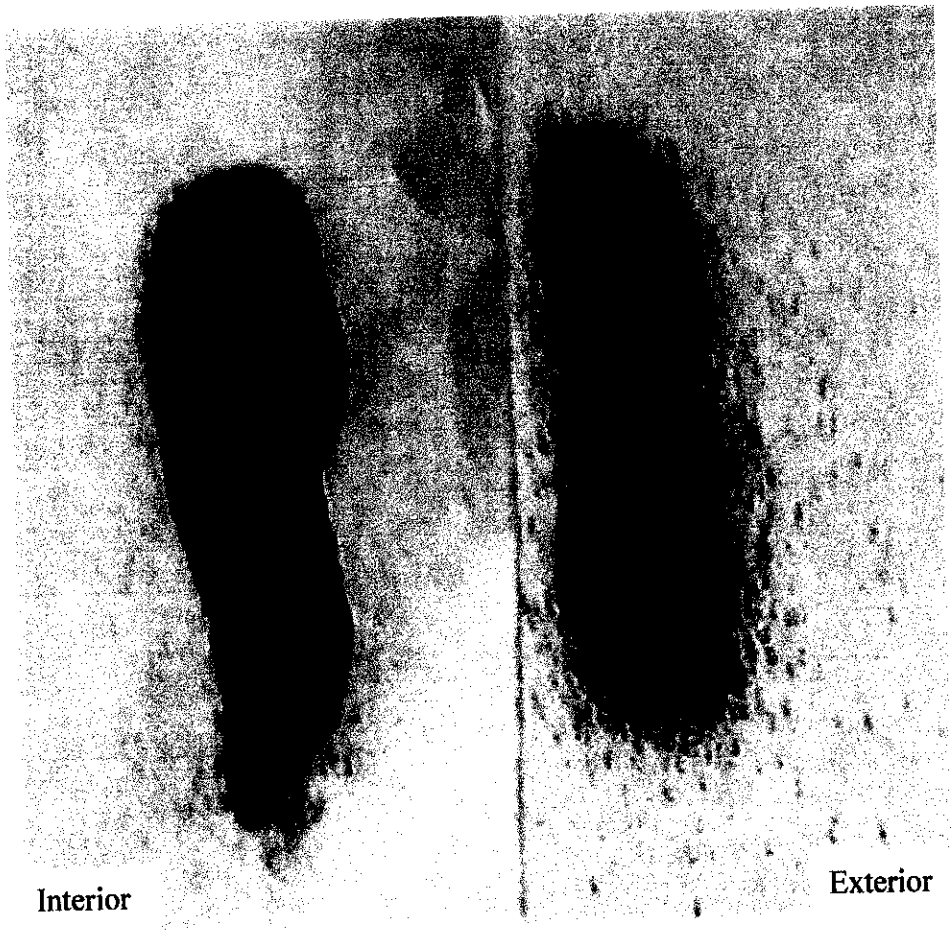

Fig (4.8). *Digital photo for the interior and exterior layers of the powder illustrated in figure (4.6)*

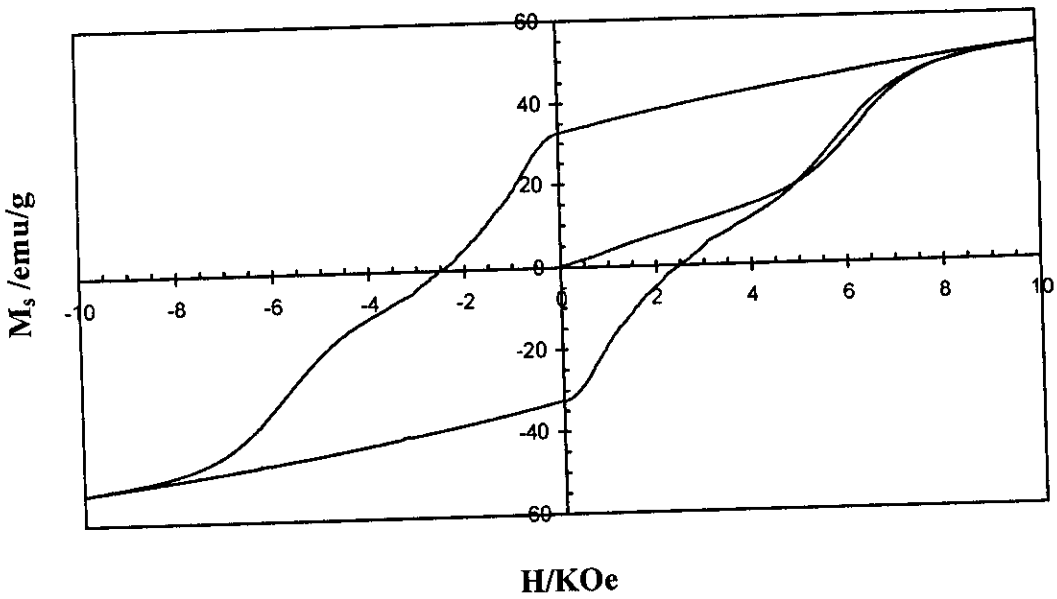

Fig (4.9) *Hysteresis curve of the powder represented in figure (4.5) annealed in the absence of oxygen*

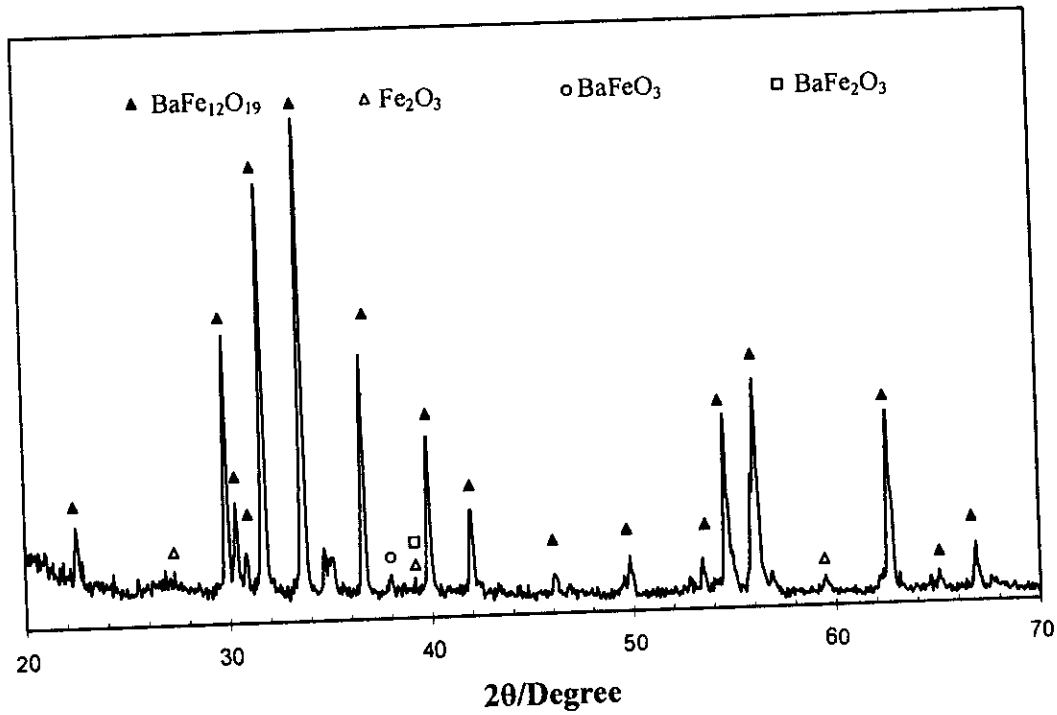

Fig (4.10) *XRD pattern of the powder illustrated in figure (4.9)*

After co-precipitation the powder was grinding (soft hand grinding) using a ceramic mortar, then sieved and six classified into six sets according to their particle sizes and size distribution as listed in table (4.2).

The heat treatment of the classified powders was carried out in the temperature range from 800 to 1000 °C to select the suitable treatment temperature for each particle size and size distribution. Taking into consideration the 10 previous preparation parameters listed in section 4.1.

The hystersis loops for the six mentioned powders are illustrated in figures (4.11~4.16) respectively. One notices that, figure (4.11), for rough powder which contains a wide particle size and size distribution recorded low coercive force (3.85 KOe) and saturation magnetization (54.5 emu/g) similar to the grinded rough fine powder ,see figure (4.3). This is because, both powders contain fine and multi phases particles, they are similar in morphology . By removing the fine powder (less than 45μm), see figure (4.12), the magnetic behavior improved leading to an increase in both of saturation magnetization and coercive force at the same time. Accordingly by reducing the size distribution to narrow range 200~100 and more narrower 100~75 μm figures (4.14) and (4.15) respectively , demagnetization curve extended to large coercivity and disappear of kink in B-H curve ,subsequently they illustrate magnetic properties with maximum values of H_c and M_s . By increasing the particle size up to 200 μm, coercive force starts to decrease again as a result of the little reaction inside the larger size particles and/ or the aggregation of the finest powder leading also to reduce oxygen penetration as mentioned before. In addition the fine powder

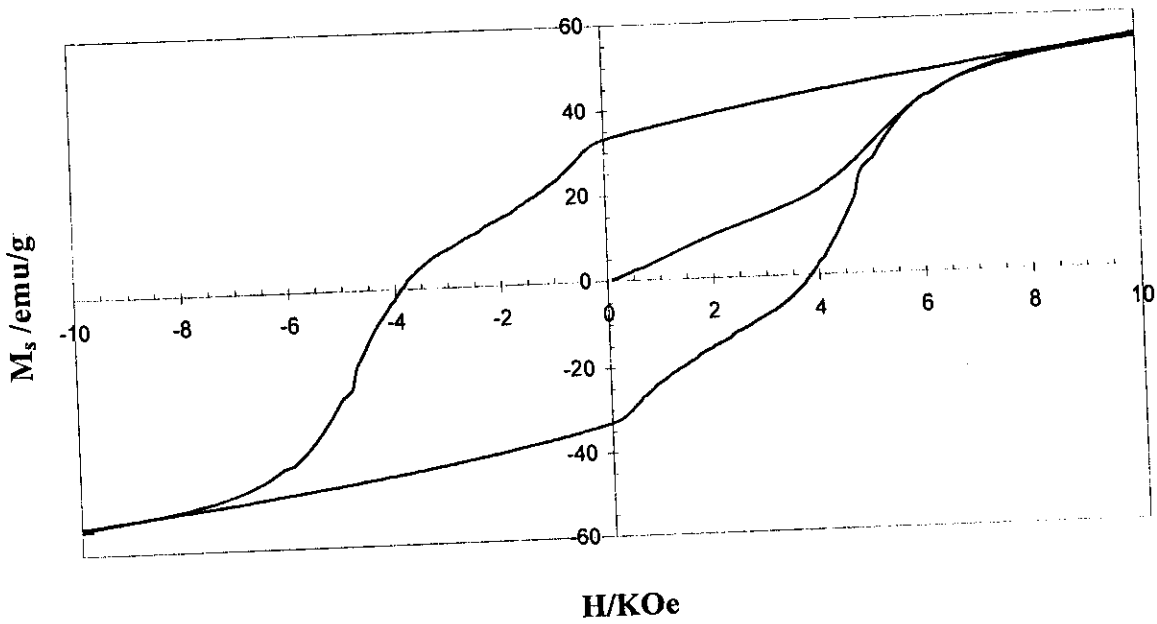

Fig (4.11) *Hysteresis loop for rough powder*

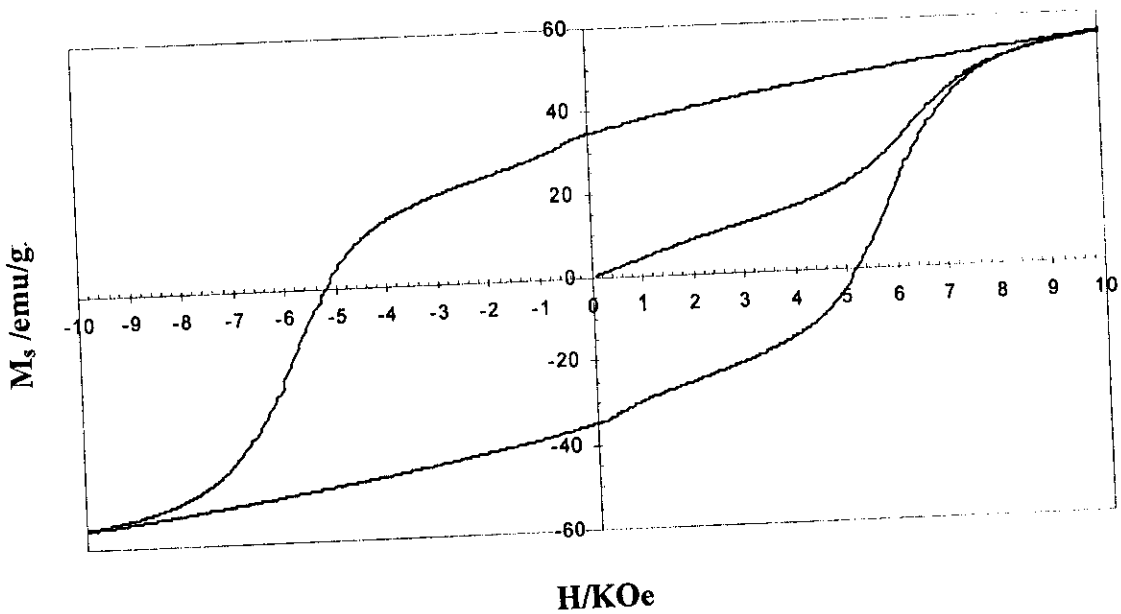

Fig(4.12) *Hysteresis loop for rough powder after removing powder less than 45μm*

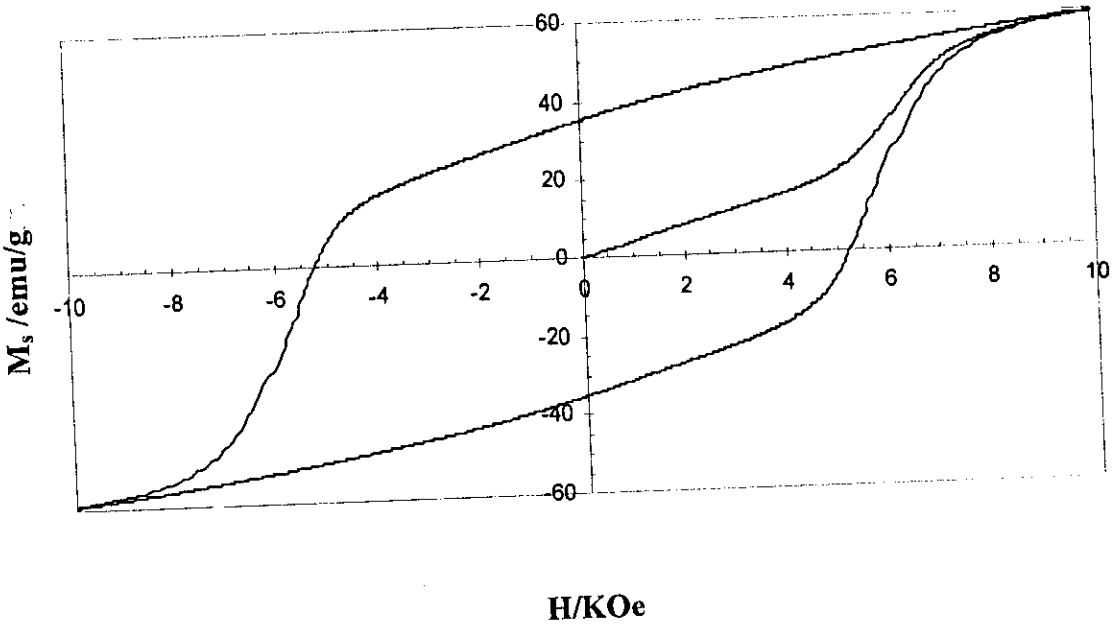

Fig (4.13) *Hysteresis loop for the powder with particle size higher than 200* μm

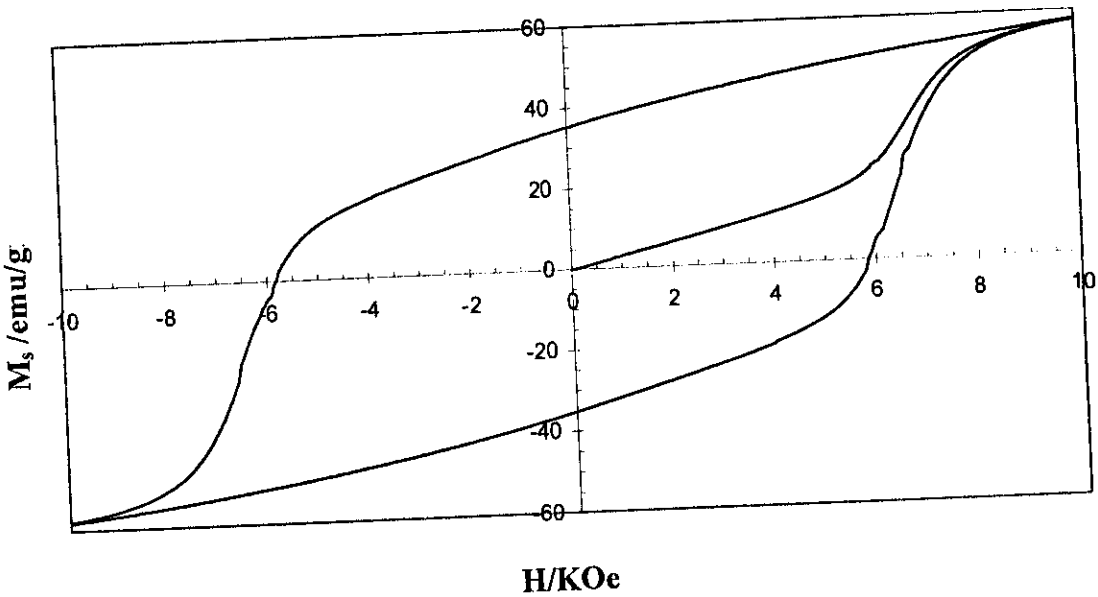

Fig (4.14) *Hysteresis loop for the powder with* particle size 200~100 μm

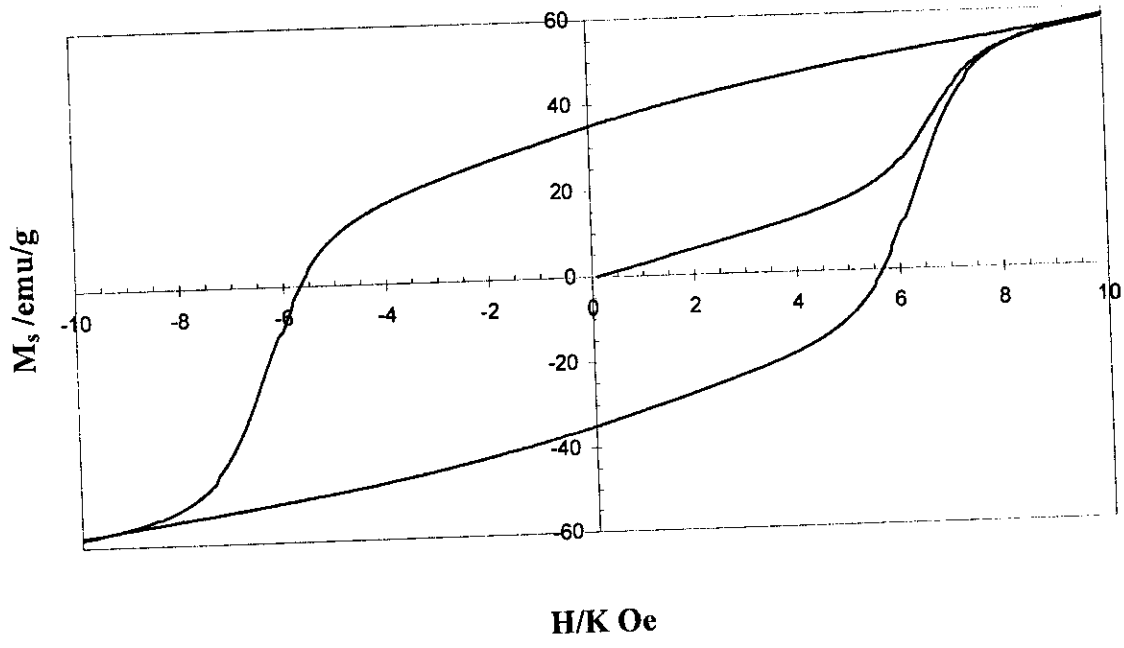

Fig (4.15) *Hysteresis loop for the powder with* particle size 100~75 μm

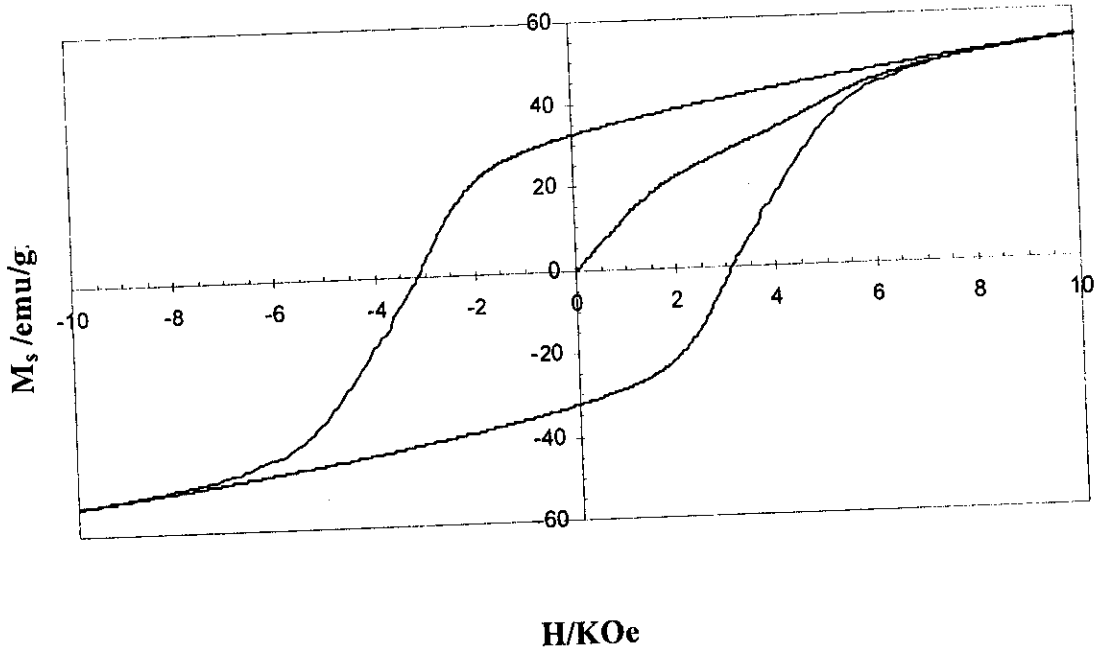

Fig (4.16) *Hysteresis loop for the powder with particle size Less than 45 μm*

illustrates the lowest coercivity and saturation magnetization because of particle aggregation and the oxygen deficient

In order to explain the magnetic behaviors according to the change in the particle size and size distribution. Firstly as mentioned, barium hydroxide and ferric hydroxide have different solubility which leading to precipitate of both hydroxide in different rates in water and subsequently results in a change of the ratio of Ba / Fe in the precursor than the starting one .The Fe/Ba molar ratio checked in the precursor for rough, 200~100, and less than 45 μm powders by using (EPMA). The results indicate that there is no any significant change of the values of n, they illustrate meanly the same initial value n=11. However the fluctuation in n increases by reducing the particle size or increasing the size distribution. They strongly depend on the preparation method and grinding level of the powders. In the case of our samples and powders, the average values of n were estimated for the samples under investigation, listed in table (4.3).

Photomicroscopic examination was used to clarify the nature of the powder morphology of powders rough, 200~100,and less than 45μm, before and after heat treatment, Figures 4.17, 18, and 19 respectively. In the case of rough and 200~100 μm, it is clear that there is no any significant change in the particle size by heat treatment. The rough powders figure (4.17) exhibits a wide particle size distribution and different degrees of particle aggregation, it increases with fine zone and there is no change in large particle size zones. In particles aggregates zone (fine particle zones), oxygen can not penetrate these zone ,whereas in zones having larger particles, the oxygen level surrounding particles is sufficient . Therefore, it is expected that sufficient oxygen will not be available at the high

Therefore, it is expected that sufficient oxygen will not be available at the high aggregation zones compared to the others, results in poor particles and inhomogeneous powders with second phases. In the case of 200~100 μm powders, high dispersibility and porosity were recorded and consequently homogeneous powders having high coercivity were formed [4]. In addition the fluctuation in the molar ratio n can be explained according to the powder morphology. The fine powder area seems to show higher fluctuation in n values than the large size area. This may result from much grinding of the powder, which separates the starting materials from each other to fine particles with different concentration of Fe and Ba atoms, so the mixing of starting materials in the ionic levels , which is the essential factor of the coprecipitation method, as mentioned before will not be valid for the fine or multi size rough and less than 45 μm powders. On the contrary, for the powders with homogeneous and large particle size 200~100, good mixing will be available and consequently definite value of n (11±0.2) is recorded. In the case of finest powder, which has particle size less than 45 μm. The fluctuation in n value decreased slightly than the rough one, because it possesses narrow size distribution and more homogeneous comparing by the rough powder. From these results one can deduce that, the fluctuation in molar value n increase by increasing the size distribution or decreasing the particle size.

Differential thermal analysis (DTA) was used to detect the reaction temperatures for the rough , 200~100 and less than 45 μm precursors, DTA thermograph given in figure (4.20). Endothermic peaks located below 150 °C are recorded which is attributed to the water dehydration. The exothermic peak

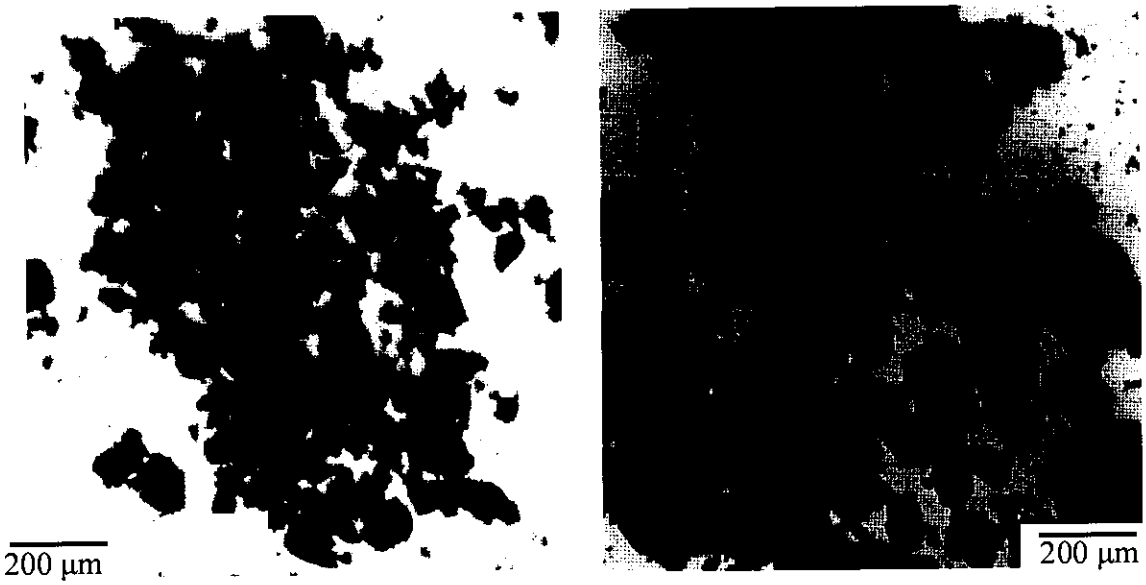

(a) (b)

Fig (4.17) *Photomicroscope micrograph for the rough powder, a -before heat treatment, b- after heat treatment*

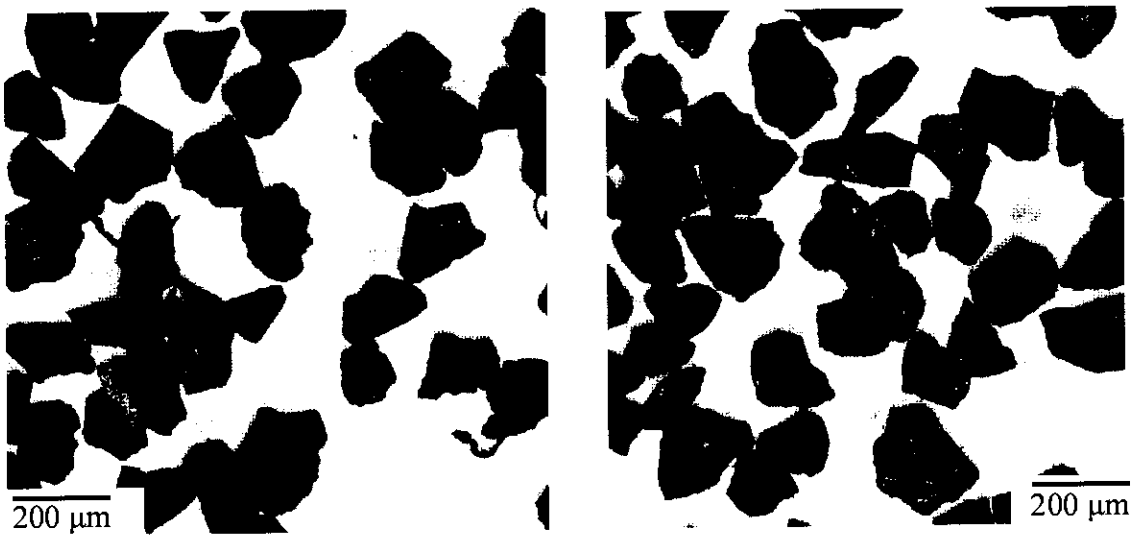

(a) (b)

Fig (4.18) *Photomicroscope micrograph for the powder with particle size 200~100μm, a- before heat treatment, b- after heat treatment*

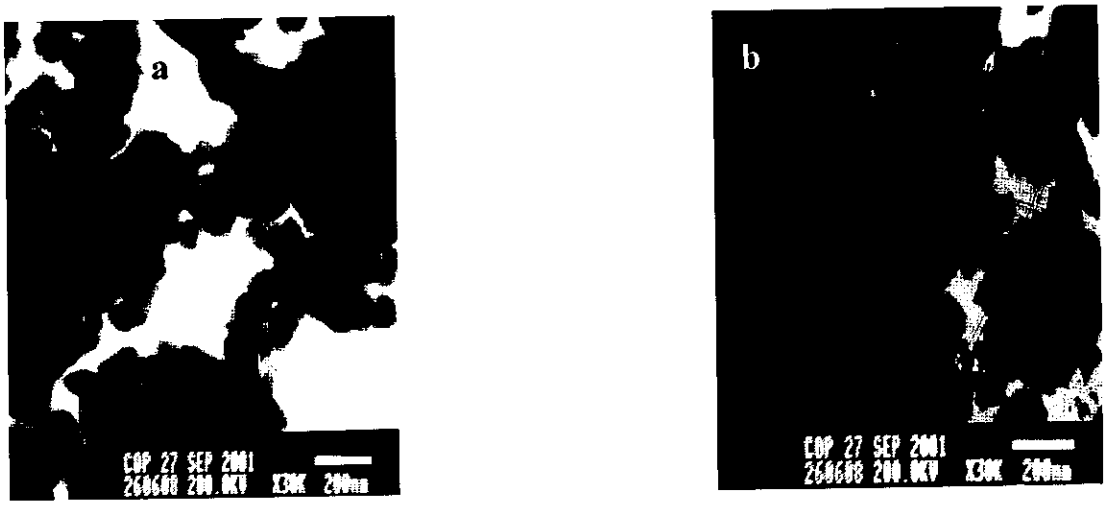

Fig(4.19). *Photomicroscope micrograph for the powder with particle size less than 45μm,a- before heat treatment ,b- after heat treatment*

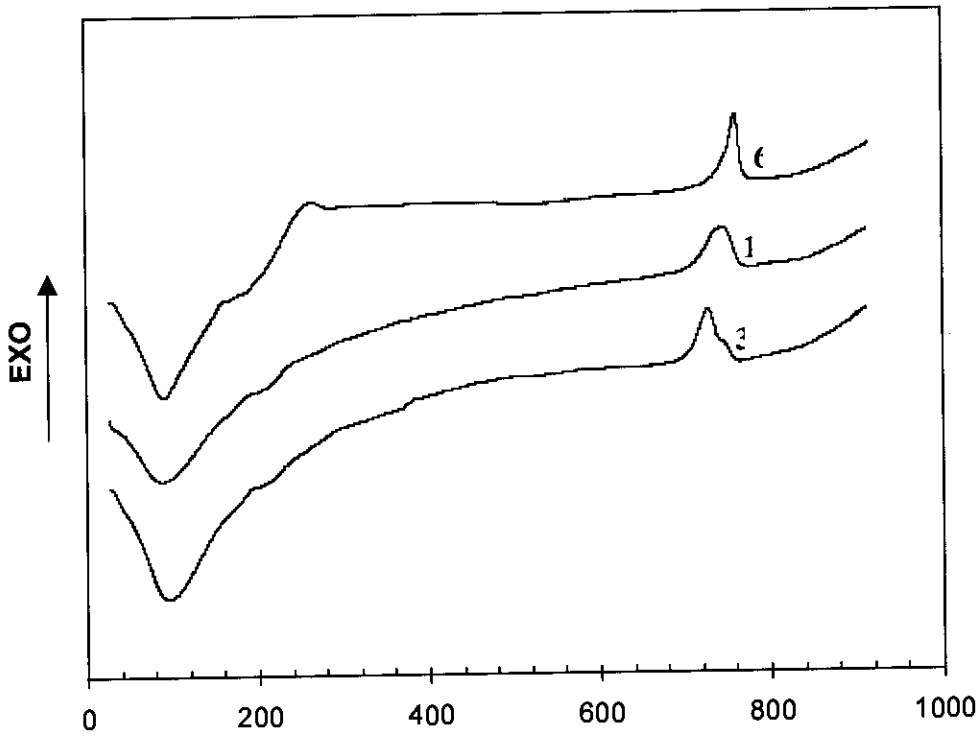

Fig(4.20) DTA graph for, (1) rough ,(3) 200~100 μm and (6) less than 45 μm particle size powders.

Powder(μm)	Molar ratio (n)
rough	11±3
200~100	11± 0.2
>45	11±2

Table (4.3). *The variation of molar ratio n with changing in particle size and size distribution, Electron probe microanalysis.*

Size distribution (μm)	T °C	H_c (KOe)	M_s (emu/g)
Rough	925	3.84	54.5
<45	925	5.15	56
<200	875	5.2	59
200-100	920	5.85	58.5
100-75	950	5.63	58
>45	1000	3.18	53.5

Tabl (4.4). *Coercive force H_c and saturation magnetization M_s corresponding to treatment temperatures for the samples under investigation.*

appears around 300 °C indicating the decomposition of hydroxides and the formation of crystalline oxides [11,19]. It is reported that barium ferrite phase starts to form at 700 °C , and a nearly single phase material can be obtained after annealing at 900 °C or above .In the temperature range 700-800 °C , three distinguished exothermic beaks appeared clearly at 735, 754, and 763 °C for the rough ,200~100 and less than 45 μm powders respectively . The difference in reaction temperatures is attributed to the different natures of the precursors, the powders having larger particles and narrow size distribution are more homogeneous and possess good mixing of the starting materials, high porosity and saturated oxygen distribution as mentioned . This reflects that crystallization can occur at relatively low temperatures [25]. The finest powder which has narrow size distribution and small particles demonstrates a higher reaction temperature in spite of its homogeneity and reasonable molar ratio than the rough powder. This is attributed to, firstly the degree of mixing level for the starting materials became poor after grinding, and secondly the low porosity with high aggregation before and after annealing as seen in figure (4.19), reduced more amount of oxygen inside the aggregated powder than the surface. Similar to the rough powder section 4.2 figure (4.8). It is noticed that the surface of the aggregated powders was more darkly brown than the interior owing to the different concentration of ferrite due to the deficient of oxygen beside the unsimilarity of oxygen distribution . The results explain why little successes accompany the formation of barium ferrite from fine powders. In the case of large particle size and narrow size distribution powder ,the morphology of the

powders was recorded using digital camera to distinguish between interior and exterior layers of the powder aggregates and compare with the rough or fine powders, figure (4.21). There is no any significant difference in the particle morphology or color was recorded as an evidence for the homogeneity of the powder. In addition, the high porosity of the powder enhances the reaction to occur completely at lower temperatures .

After photomicroscope,EPMA, DTA, and digital camera examination, it became easily to understand the magnetic behavior for the present samples.

Large particle size or narrow size distribution always exhibit a strong magnetic properties than small or multi size distribution powders due to the homogeneity , porosity , lower reaction temperature and the effect of oxygen inside the powders . Besides these the higher coercivity of large particles could be interpreted also to their individual porosity of the particles.

The recorded H_c and M_s for each powder at the appropriate treatment temperatures and 10 KOe magnetic field are listed in table (4.4). The minimum values of H_c and M_s recorded for the rough and finest powders which contains a wide of particle size distribution. Ferromagnetic material exhibits superparamagnetic behavior and affecting the magnetic characteristic at such a refined crystalline size [44].

The maximum coercive force and saturation magnetization recorded for 200~100 μm powder ,regardless of its particles size is about 200 times larger than the domain size for the hexagonal barium ferrite phase , which lie in the range of 0.2~1 as reported [17] . Higher than 200 μm powder figure (4.13) possesses higher magnetization than 200~100μm , which is attributed to the

increase in the crystallinity of barium ferrite with increase of particle size [27] and another case is the decrease of the number of superparamagnetic particles which can explain the dependence of coercivity on the particle size too.

From these results, it is concluded that thermal fluctuation (size distribution) and may be lattice defect introduce by milling rather than the particle size greatly affect the magnetic properties of barium ferrite powder .

By controlling particle size distribution and the other preparation parameters, $BaFe_{12}O_{19}$ phase have been successfully prepared by co-precipitation method with good magnetic properties .

SQUID magnetometer was used to select the optimum properties of the final powders where the isotropic field of hexagonal barium ferrite phase is about 17 KOe and saturation magnetization at room temperature 72 emu/g [58] . Figure (4.22) shows a comparison of the hysteresis curves for the rough and 200~100μm powder. The high coercivity powder recorded a saturation magnetization after the isotropic field 71 emu/g and H_c 5.85 KOe. According to the discussion given above, the magnetic properties of the sample 200~100μm are basically determined by a geometrical factor of particle distribution. The homogeneous distribution of the coarse particles with narrow size distribution provides large porosity in the aggregates, which help to supply enough amount of oxygen to mix starting materials in the ionic level for the crystallization of stoichiometric $BaFe_{12}O_{19}$ phase. The recorded saturation magnetization and coercivity are very close to the theoretical values (H_c=6.7 KOe, M_s= 72 emu/g) according to the Stoner-Wohlfarth (SW curve) [80].

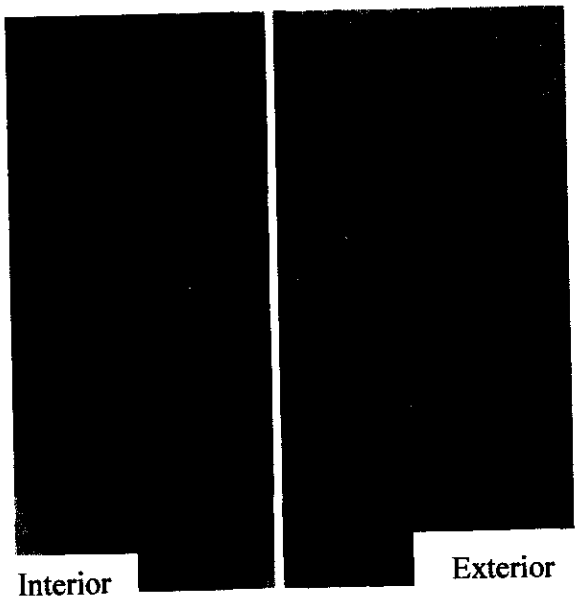

Fig (4.21). *Digital photo for the interior and exterior layers for 200~100μm powder illustrated in figure 4.14*

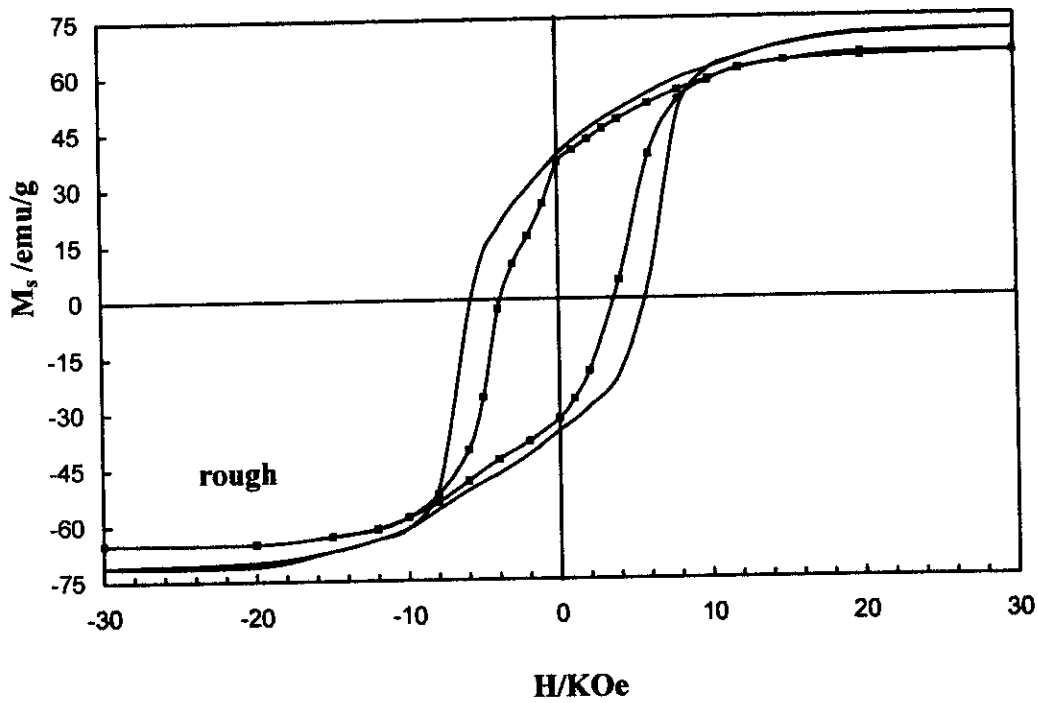

Fig. (4.22) Hystersis loop for rough and 200~100 *μm powder recorded by SQUID magnetometer up to 30 KOe*

4.3 Characterization of Rubber- Ferrite composites

Barium ferrite powder with 45~200μm particle size, 5.2 KOe coercive force and 57 emu/gm saturation magnetization was chosen as a filler for preparing rubber-ferrite composites, see table (4.4). The microstructures were carried out by SEM microscope to identify size, shape and distribution of ferrite particles in rubber matrix. In a free state figure (4.23), the ferrite particles are irregular in shapes , have smooth surfaces and sharp edges .According to SEM micrograph , the majority of the particles lie in the range of 50~100μm . Few particles exceed 150μm in the size are present, the other particles less than 45μm (25<D>45μm) arise by the fragmentation of large particles. Very fine particles do not appear after powder sieving. In the case of rubber – ferrite composite (RFCs) , figure (4.24) represents the SEM micrographs for 30, 90 and 120 phr ferrite loading. It is clear that, ferrite particles are homogenously distributed in the rubber matrix, and new some fine particles appeared again due to larger particles fragmentation by rubber remilling without any change of the particles morphology ,see figure (4.23) . The particles appeared to be isolated by rubber layers from each other even in the higher ferrite load (120 phr) .

Figure (4.25) illustrates X-ray diffraction pattern for the used ferrite. The pattern exhibits 4 reaction products, namely, hexagonal $BaFe_{12}O_{19}$ besides parasitic four phases, $Ba_5Fe_{14}O_{26}$, $BaFe_2O_4$, and Fe_2O_3, their appearance depends on powder porosity and oxygen deficient around the particles.

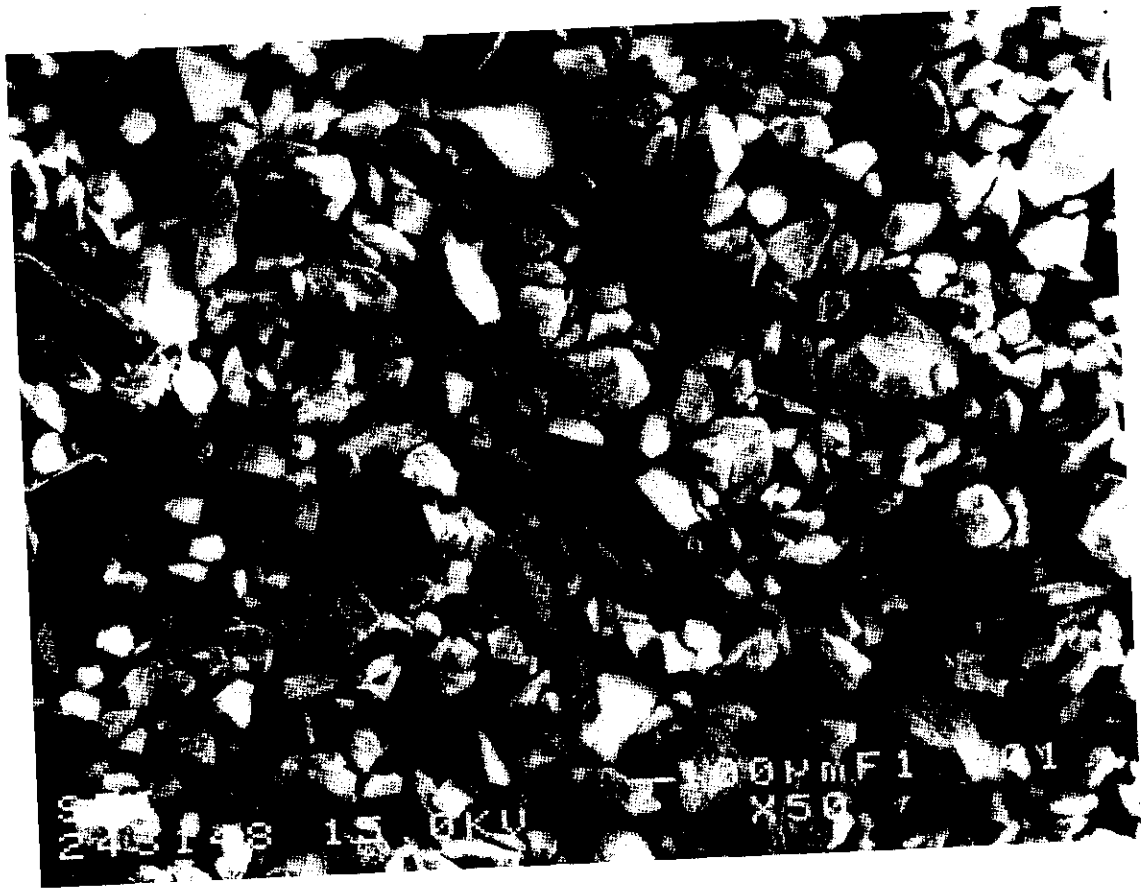

— 100µm

Fig.(4.23) *Scanning Electron Micrograph for barium ferrite powder in a free state*

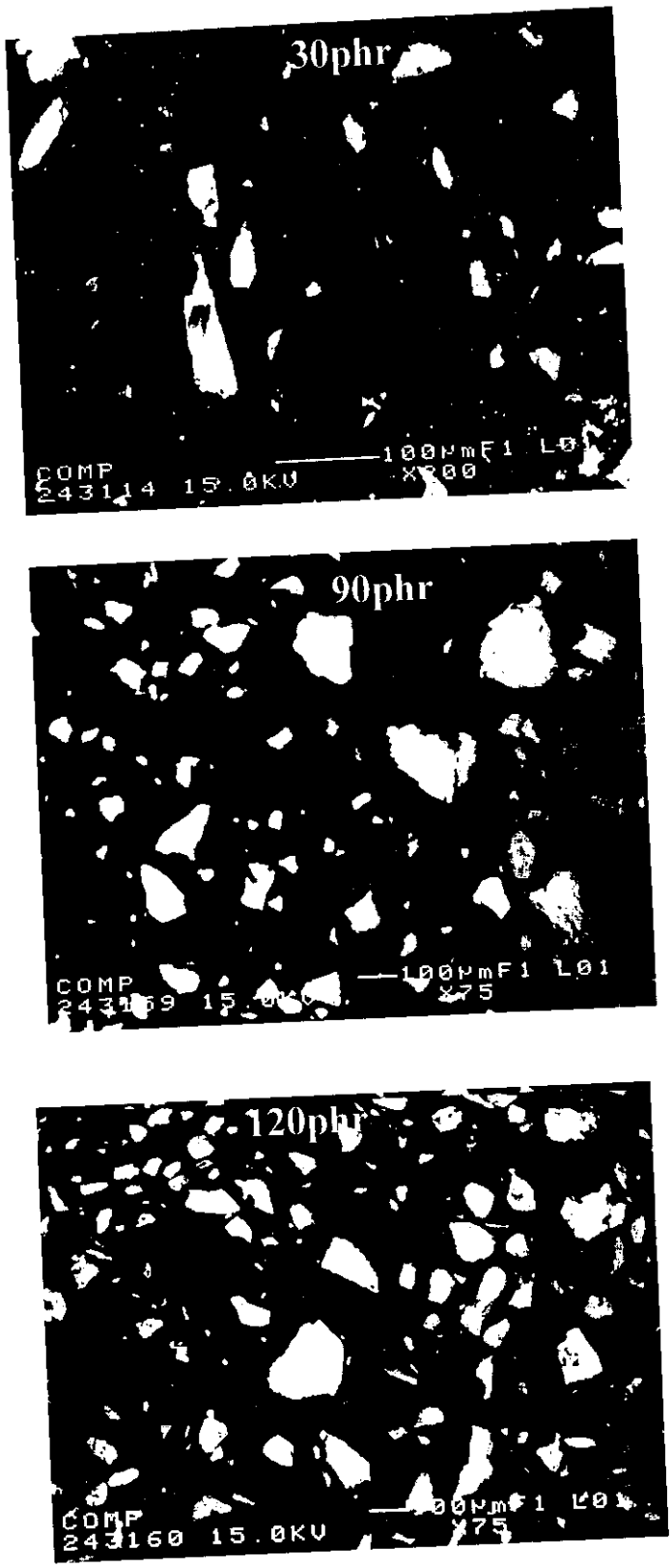

Fig (4.24) Scanning *electron macrographs for rubber-ferrite composites*

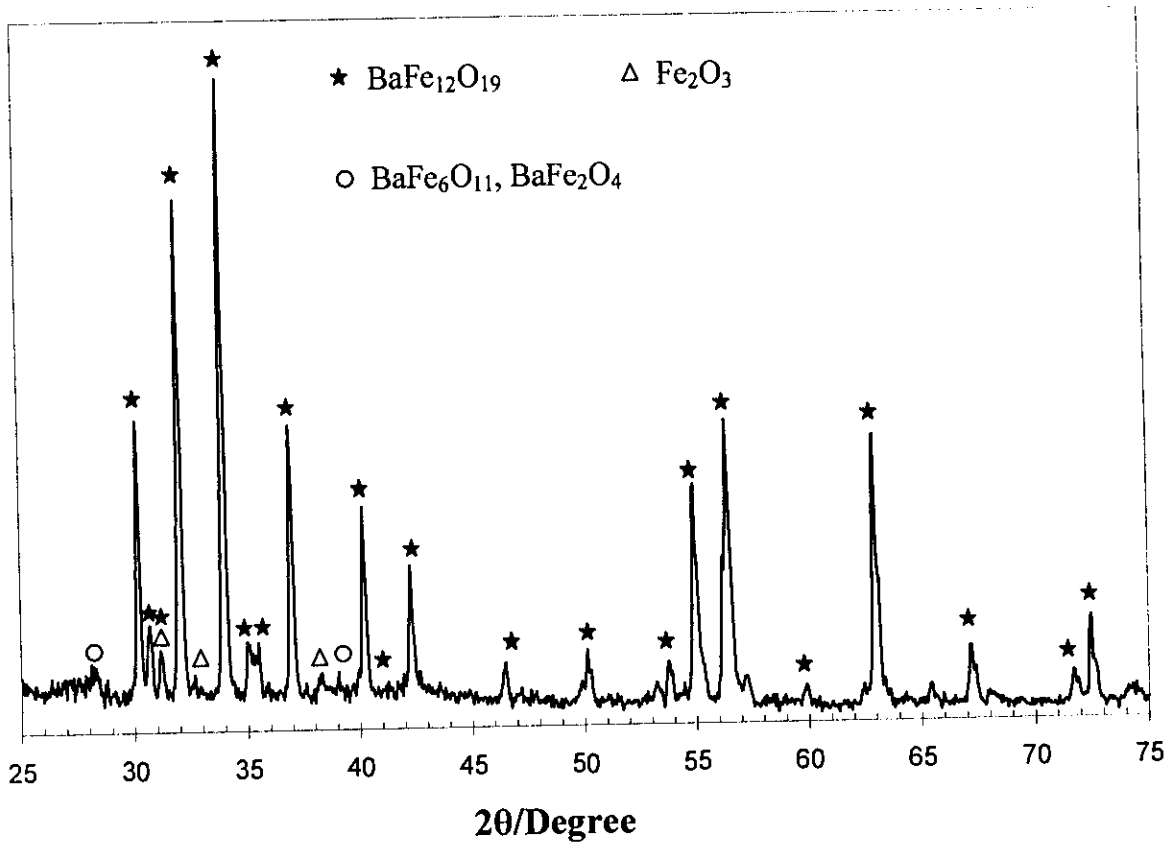

Fig (4.25) X-*ray diffraction pattern for the barium ferrite powder mixed with rubber*

4.3.1. Magnetic Properties of RFCs

Magnetic properties were carried out for rubber and rubber-ferrite composites in SQUID magnetometer up to 30 KOe and listed in figures (4.26-31). It can be observed that the magnetization increases by increasing ferrite content. No contribution from vulcanized rubber and /or other additives in the magnetic behavior for the composites, where rubber matrix are diamagnetic materials as seen in figure (4.26). From these curves the values of saturation magnetization and coercivity for the samples with different loading were determined and plotted in figure (4.32) against the mass fraction of the filler. It indicates that H_c is almost independent of the mass fraction at low ferrite loading in contrast with the previous works [34,44,46], and only the major effect of loading is to increase the remaining magnetization. The change in H_c with ferrite fraction can be explain as follows; at low level of ferrite loading, the saturation in H_c can be attributing to; (1) the desegregation of the filler caused by removing the fine powders prior to mixing, (2) the high degree of mixing which is a critical factor in controlling the magnetic and mechanical properties of polymers bonded magnets [49], and (3) the fact that the present magnetic particles as a filler are relatively large in size, randomly oriented, uniformly dispersed and isolated from each other even at high concentration 120 phr. The later will reduce the surface energy of the particles, which controls the mean distance separate particles from each others during mixing in addition to the irregular shape of the particles offers low surface area than the spherical particle. So, there is no tendency to form agglomerates in the RFCs even at a relatively high loading level. At a critical

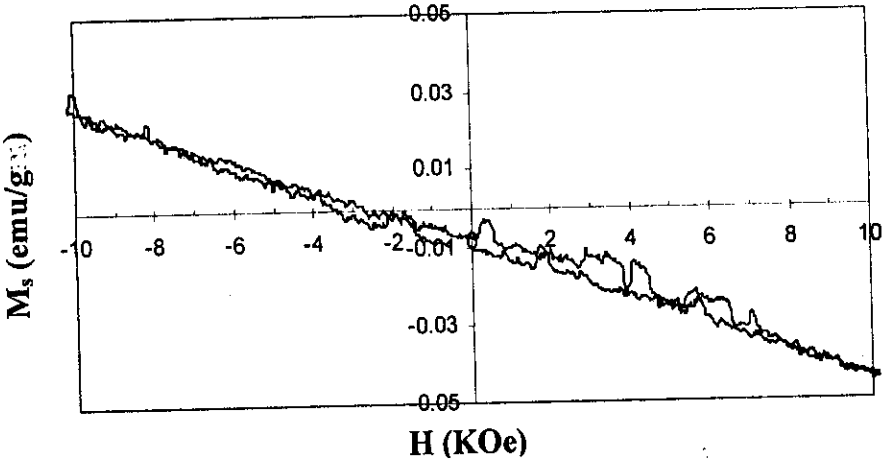

Fig.(4.26).
NR Rubber

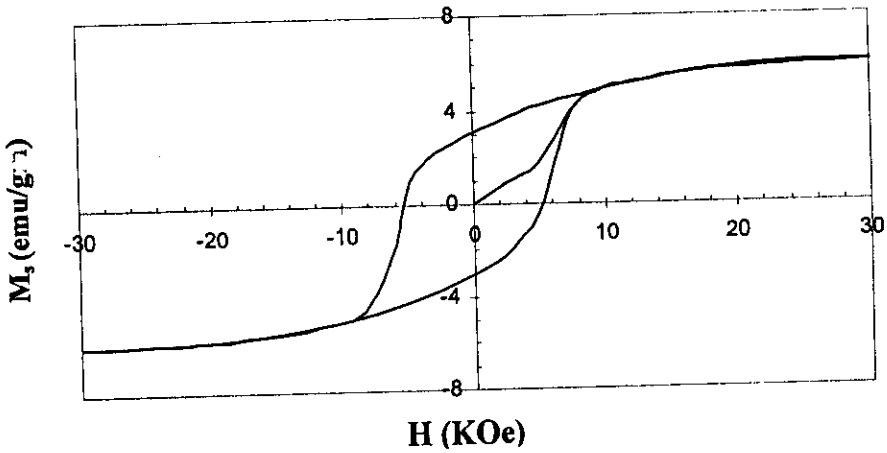

Fig.(4.27).
10 phr ferrite

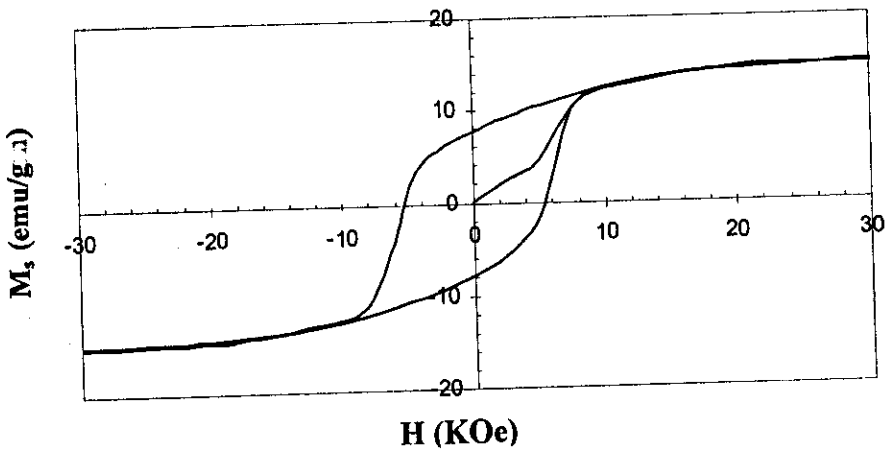

Fig.(4.28).
30 phr ferrite

Hystersis loops for NR rubber and rubber- ferrite composites

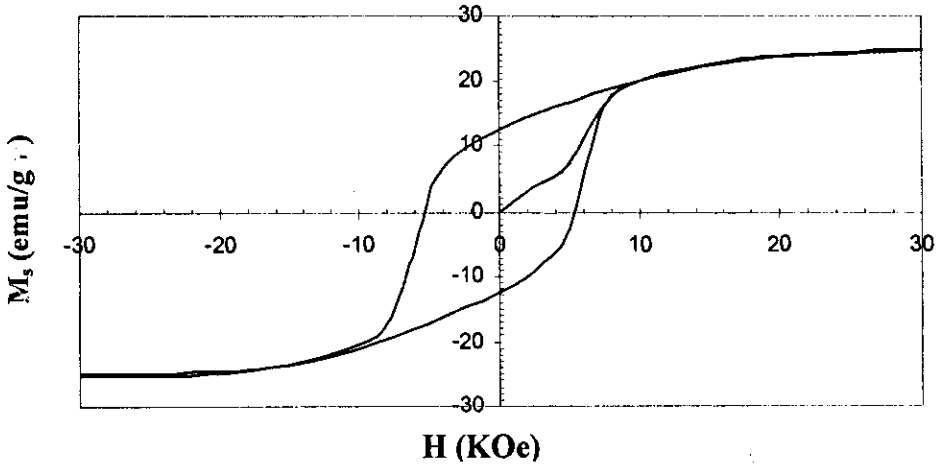

Fig.(4.29).
60 phr ferrite

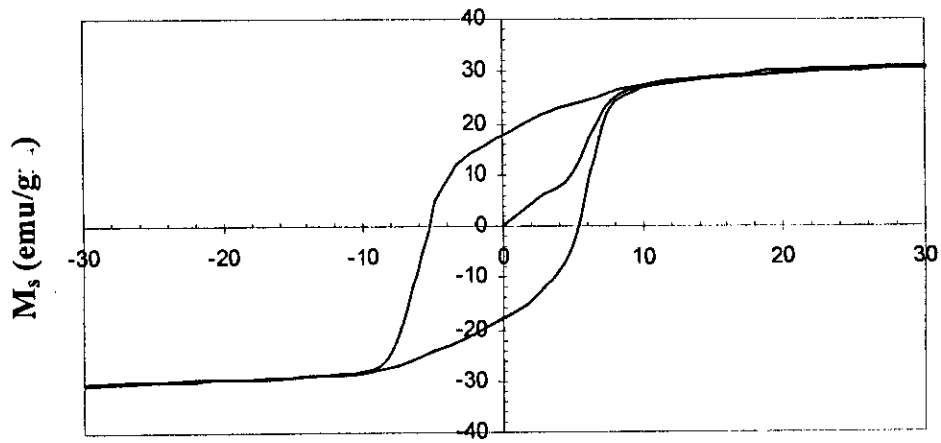

Fig.(4.30).
90 phr ferrite

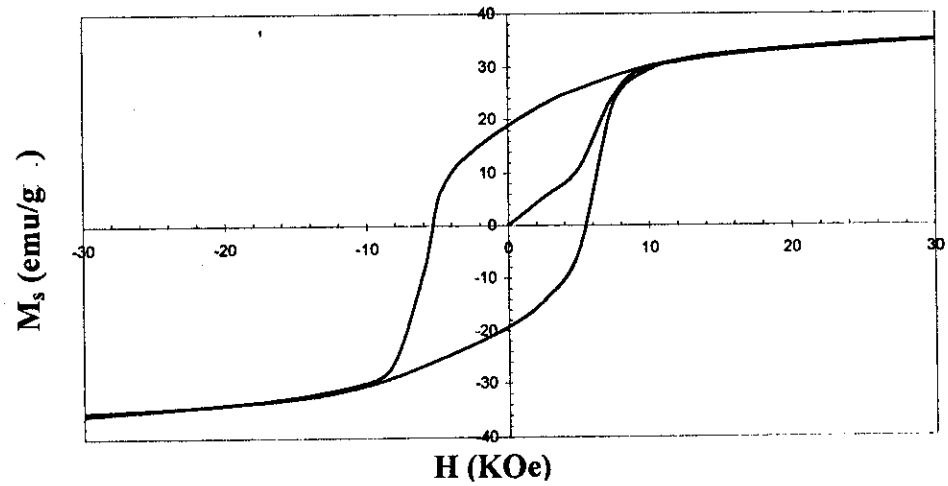

Fig.(4.31).
120 phr ferrite

Hystersis loop for NR rubber- ferrite composites

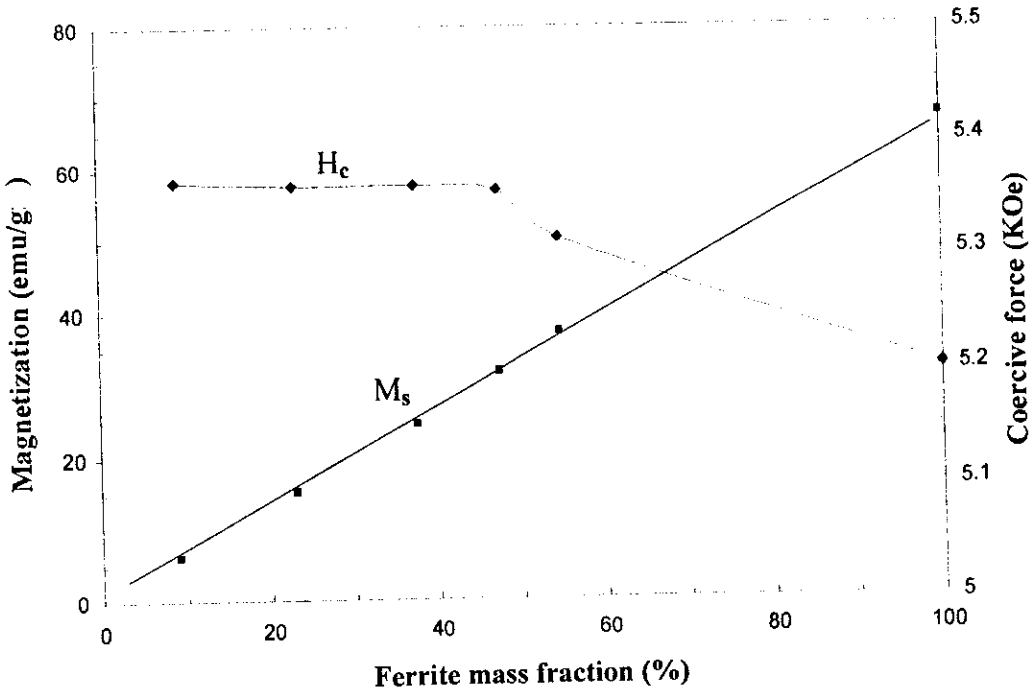

Fig.(4.32). *The variation of saturation magnetization (M_s) and coercive force (H_c) as a function of the mass fraction of ferrite*

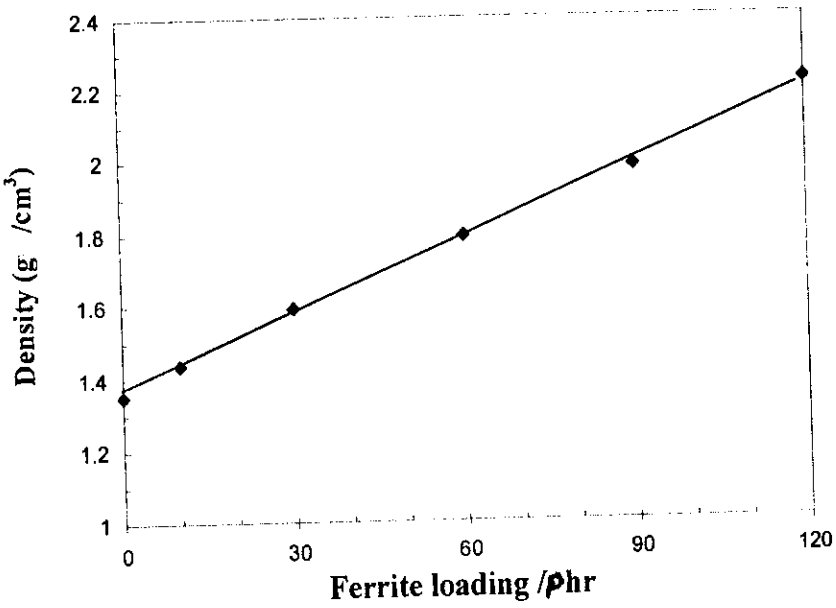

Fig. (4.33). Variation of rubber-ferrite composites density with ferrite loading

loading about 100phr the H_c starts to decrease due to the increasing of magnetic interaction between the ferrite particles as the mean interparticle separation distance decreases. The magnetic pathways in polymers-bonded magnets critically depend on the relative association of the magnetic fillers and their level of dispersion. Particle-particle interaction become important above critical loading [81]. In the present RFCs ,Particle–particle interaction becomes important above a barium ferrite 100 phr loading about (50%) volume fraction. It tend to enhance the magnetic properties of the composites .

The change in both of the density and the saturation magnetization of RFCs result from the weight addition of filler to the rubber matrix. The magnetization values of the RFCs from M_s Value of the ceramic sample have been estimated using the following simple mixture equation ;

$$M_{rfc} = M_f W_f + M_r W_r$$

Where M_f and W_f are the saturation magnetization and weight fraction of ferrite powder respectively, M_r and W_r are saturation magnetization and weight fraction of rubber matrix respectively . Since the rubber matrix is nonmagnetic, this equation can be reduced to the following form;

$$M_{rfc} = M_f W_f$$

Which represent linear dependent for the composite magnetization on ferrite mass fraction, figure (4.32).

The density of the composite varies linearly with the volume fraction of barium ferrite according to the formula,

$$\rho_{rfc} = \rho_r + (\rho_f - \rho_r)\phi_f$$

Where ρ_{rfc} is the density of RFCs , ρ_r matrix density and ρ_f is the ferrite density and Φ_f is the filler fraction.

Figure (4.33) shows the variation of RFCs density as a function of the volume fraction of barium ferrite. The figure indicates that composite density increase linearly by increasing ferrite loading up to 2.2 g/cm^3 at 120 phr ferrite content. The barium ferrite density was calculated using the total atomic mass of the hexagonal unit cell by using the lattice parameters as follow[82]. The unit cell density ρ of solid materials is computed through the relation

$$\rho = \frac{nA}{V_c N_A}$$

Where ; N= number of atoms associated with each unit cell, A= atomic weight, V_c = volume of unit cell, N_A = Avogadro's number (6.023×10^{23}) .

In the case of crystalline ceramic materials the ρ density may be determined using a modified form of the present equation as follows;

$$\rho = \frac{n^{`}(\sum A_c + \sum A_A)}{V_c N_A}$$

Where; n = the number of formula units' within the unit cell, ΣA_c=the sum of the atomic weights of all cations in the formula unit , ΣA_A =the sum of the atomic weights of all anions in the formula unit .

For the hexagonal barium ferrite unit cell $BaFe_{12}O_{19}$ phase,

$n = 2$ unit cell = 2($BaFe_{12}O_{19}$), figure (2.4),

($\Sigma A_c + \Sigma A_A$) = (137.34+ 55.8x12 + 15.99x19) = 1112

V_c = total volume/ 3 as in figure (4.34a)

The lattice constants a and c for the hexagonal barium ferrite powder are estimated from TEM diffraction pattern micrograph indicated in figure (4.34b).

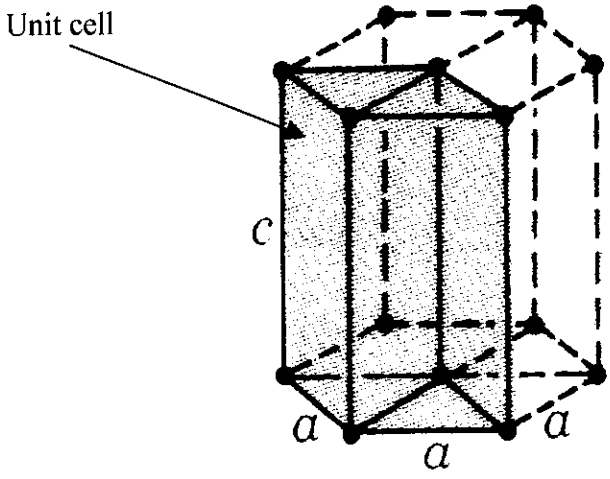

Fig.(4.34 a) .H*exagonal structure unit cell*

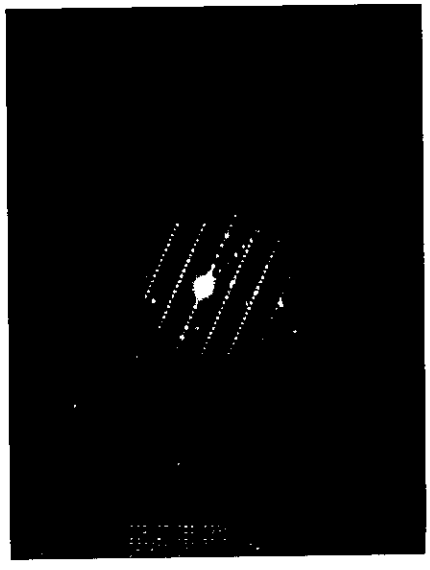

Fig.(4.34 b). *TEM diffraction pattern of hexagonal barium ferrite*

Both the lattice constants a and c equal 5.42 and 23.6 Å respectively. Their values lead to density of the free barium ferrite powder about ρ= 6.19 g/cm^3. The theoretical density (5.28 g/cm^3).

This change in density can be attributed to the difference of the lattice parameters of the present samples and for that given in literatures (a= 5.89 Å, C= 23.18 Å) . Or powder has different nature than the others.

The energy product *(BH)* is obtained by multiplying the flux density *(B)* by the magnetic field intensity *(H)* for each point of the demagnetization curve. This important quantity is proportional to the stored energy in a permanent magnet. Figure (4.35a) shows the energy product of the studied composites samples as a function of magnetic field intensity (H) for different phr. At a given value of H the maximum stored energy for every sample was recorded and redrew against the mass fraction of ferrite ,figure (4.35b). As expected it shows a linearly dependence of the $(BH)_{Max}$ values with the mass fraction of barium ferrite .
The maximum stored energy recorded in the present composites BH_{max} = 1.18 MGOe is higher than this given in literatures [34,46], compared by our maximum filler loading 120 phr and composite density 2.2 g/cm^3. This is due to the selection and the magnetic properties of the present magnetic powder.

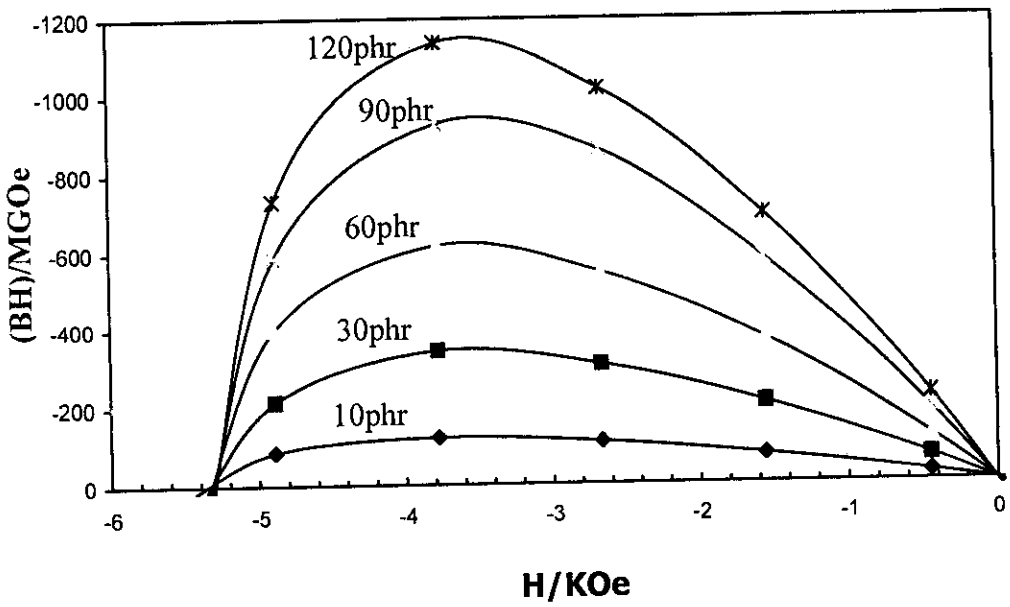

Fig (4.35a). *The dependence of the stored energy of RFCs on the magnetic field intensity*

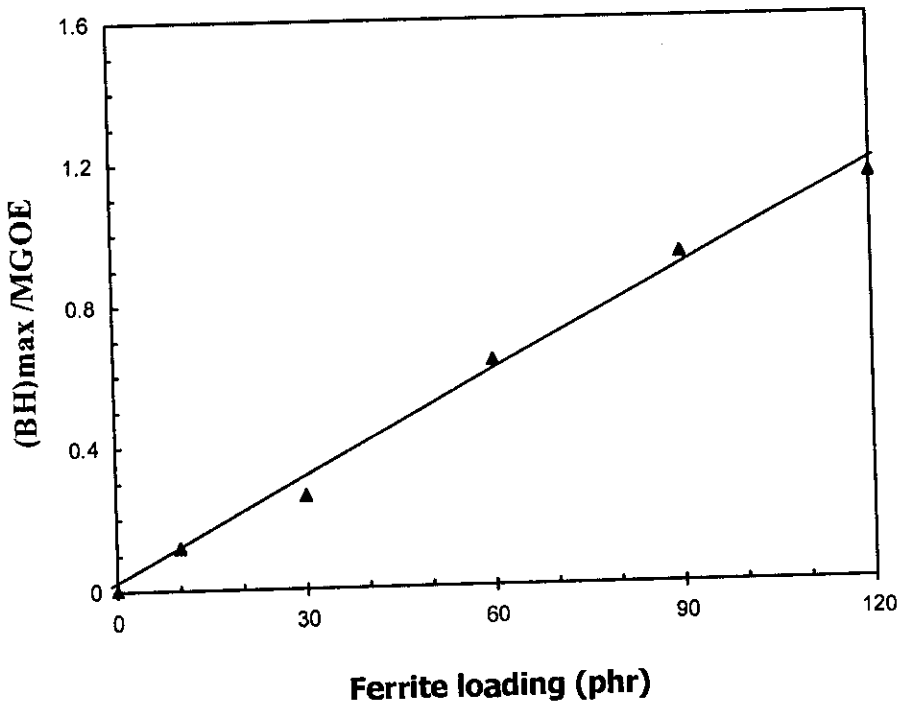

Fig.(4.35b).$(BH)_{max}$ against the ferrite loading

4.3.2. Mechanical properties of RFCs:

The creation of highly effective magnetic polymer is aimed not only to arising the level of magnetic propertied but also improving their workability ,as rather as the mechanical properties of polymer bonded magnets are strongly influenced by the size, shape, type, loading and dispersion of the magnetic filler, as well as the matrix properties and the interfacial adhesion between the filler and the polymer matrix [49,83] .In the present work, the filler particles are relatively large in size (45~200μm) having an irregular shape and untreated smooth surfaces, figure (4.23). Large size and irregular shape of ferrite particles well reduce the surface interaction among them, where they will give low wettability and adhesion with the rubber matrix at the same time [49,84].

Figure (4.36) shows the stress-strain relationship of natural rubber and rubber ferrite composite filled with different concentration of barium ferrite. It can be seen that the stress at any strain increased with increasing ferrite loading in the composite, where both stress and elongation at break decrease by increasing ferrite loading. The aging of composites for different periods at 70 °C illustrates the same stress-strain behavior, figure (4.37a-c). An irregular shift of the behavior upward or downward with increasing aging time is recorded, except after 45 days, the behavior shifts downward opposing the behavior of the untreated rubber-ferrite composites.

Figures (4.38) and (4.39) illustrate the variation of tensile strain and stress , at break point , for unaged and aged samples with increasing the barium ferrite content. Both of them decreases with increasing the ferrite powder in the rubber matrix. The decrease is more drastically at low ferrite loading ,where at high

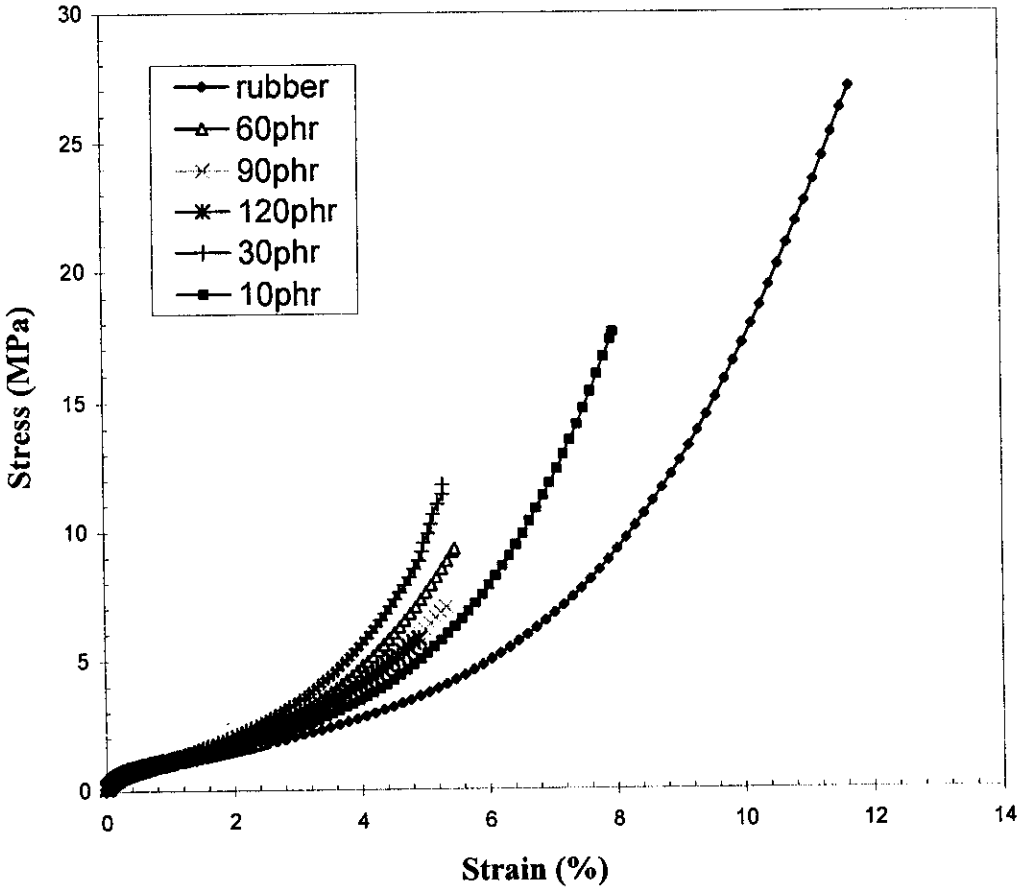

Fig (4.36) *Variation of tensile strain as a function of tensile stress for RFCs at different ferrite loading*

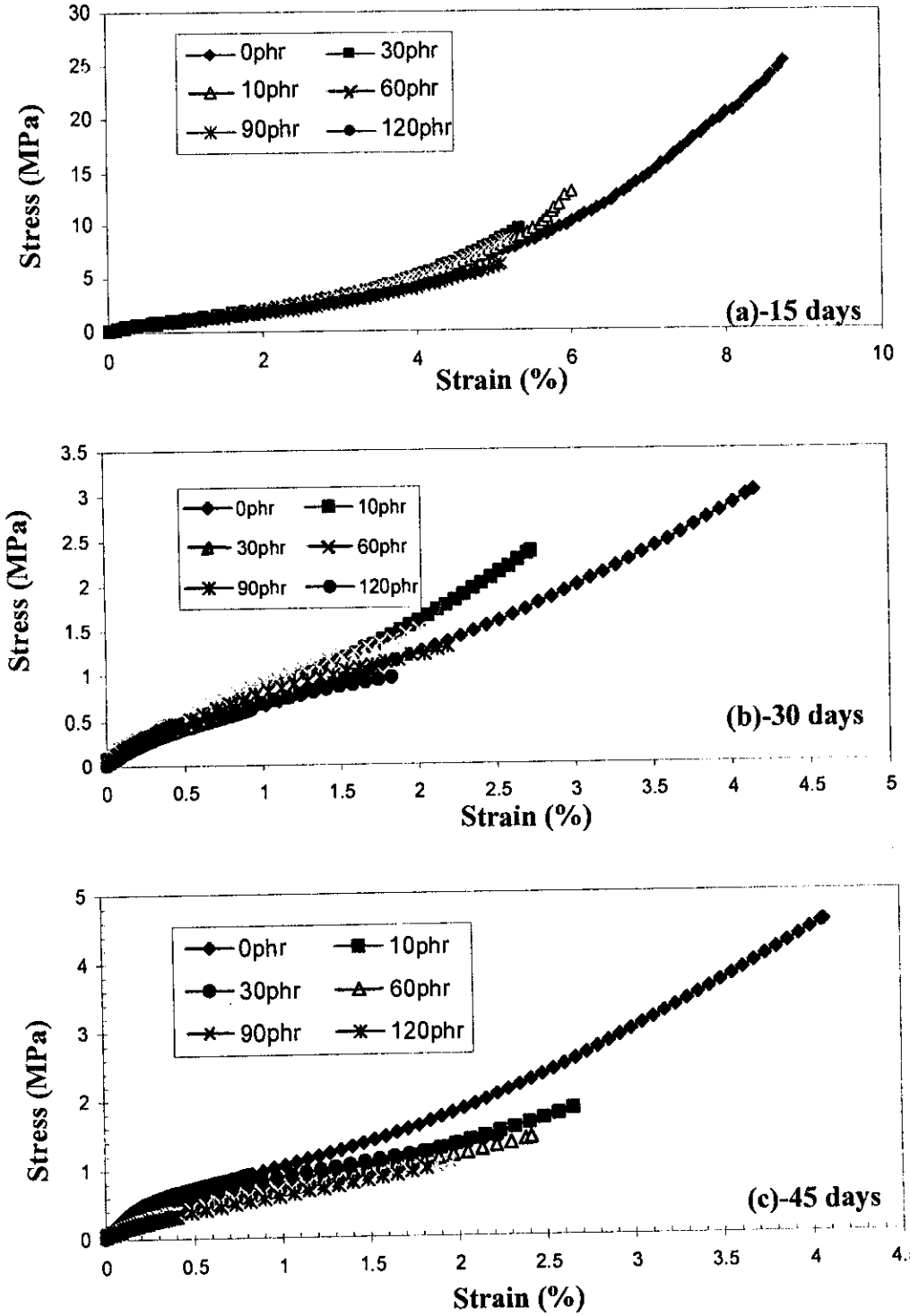

Fig (4.37) *stress- strain relation for RFCs aged at different periods*

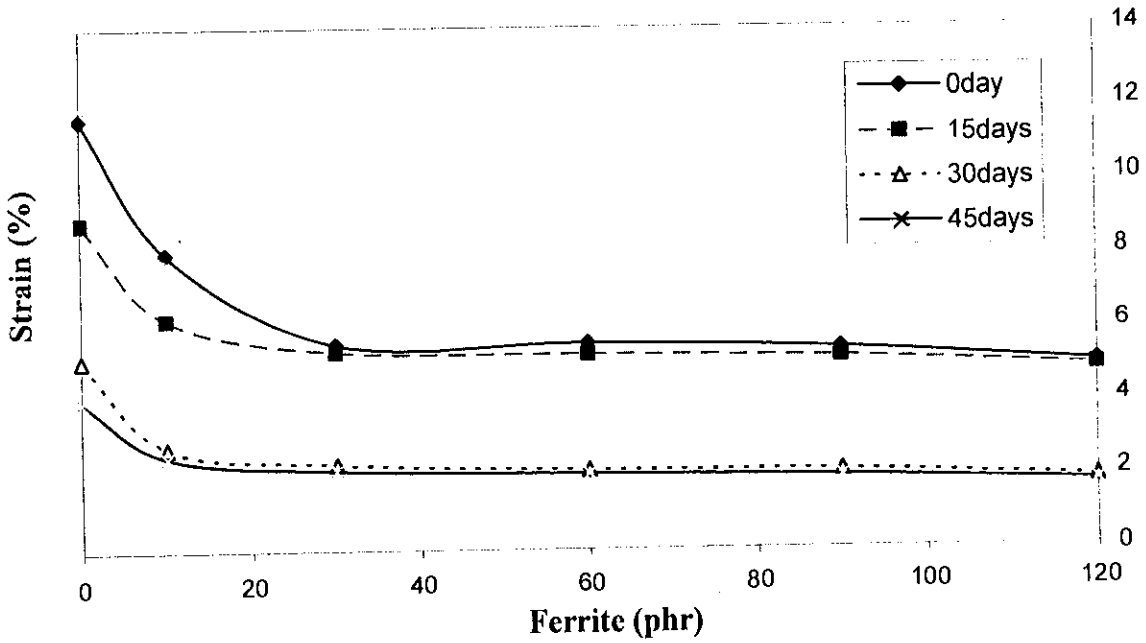

Fig (4.38) Effect of ferrite content on the tensile strain for RFCs at different aging time

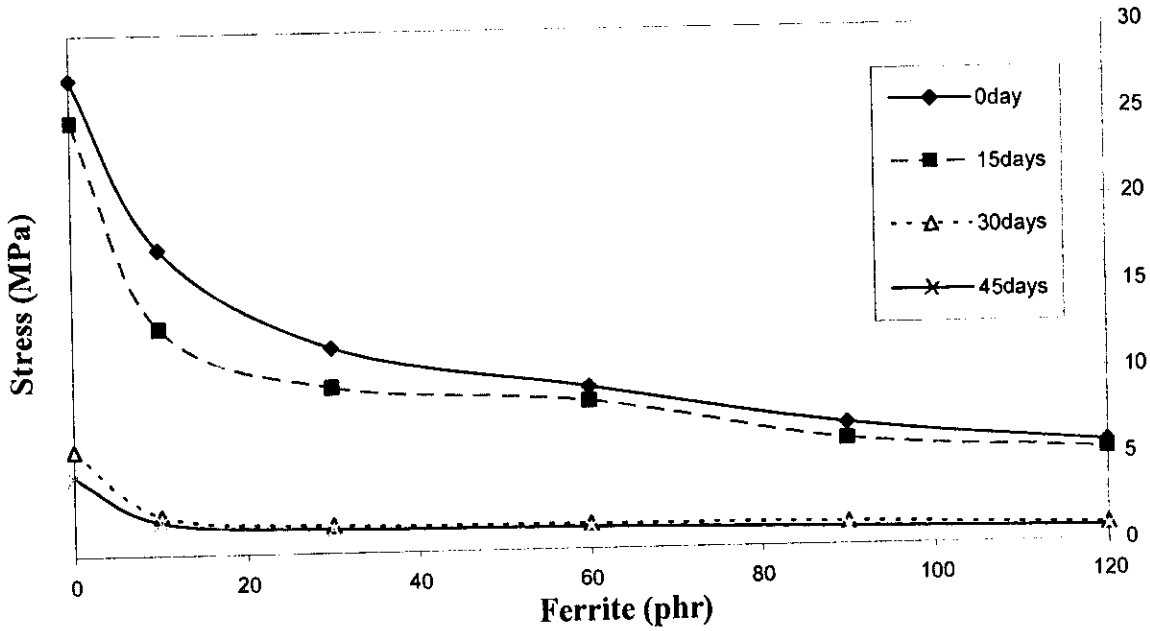

Fig (4.39) Effect of ferrite content on the tensile stress for RFCs at different aging time

loading about 60 phr the dependence of strain and stress on the ferrite loading becomes insensitive to the change in the filler content.

Figures (4. 40) and (4.41) describe the effect of aging time on both of tensile strain and stress. They decrease nonlinearly with aging time ,little variation is observed after 15 days followed by a remarkable decrease reaching an asymptotic value after 30 days ,this behavior could be explained by the following.

The degree of rubber cross-linking depends on both temperature and time of reaction [85]. At shorter time the degree of cross linking still unchanged, and after certain time the onset of reaction initiated and saturated after 30 days of aging.

Young's modulus Y were also estimated from the stress-strain curves for the present samples and illustrated in figures (4.42) and (4.43) corresponding to ferrite loading and aging time respectively. In general Y increases with increasing ferrite content ,while it decreases after 15 days with increasing aging time .The values of Y at 15 days shifts upward by increasing ferrite load which refers to the strengthing of NR/ferrite composite.

Also shore hardness was measured for the samples under investigation and illustrated in figure (4.44) and (4.45) corresponding to ferrite fraction and aging time respectively. The change of hardness increases linearly with increasing ferrite fraction in the rubber matrix. Whereas it decreases with increasing the aging time.

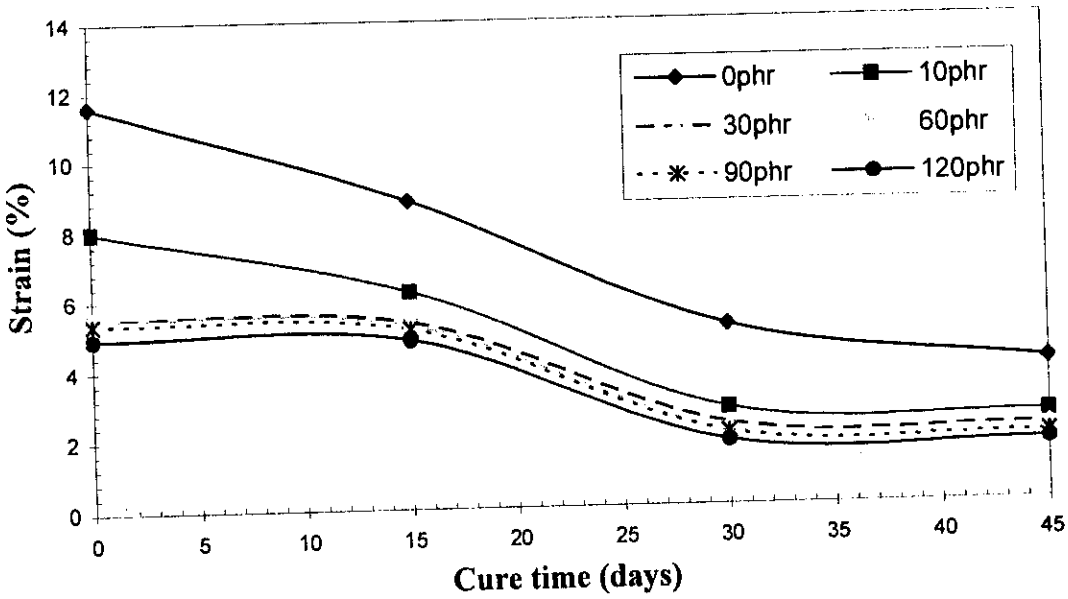

Fig.(4.40). Effect of cure time on the tensile strain of RFCs at different ferrite loading

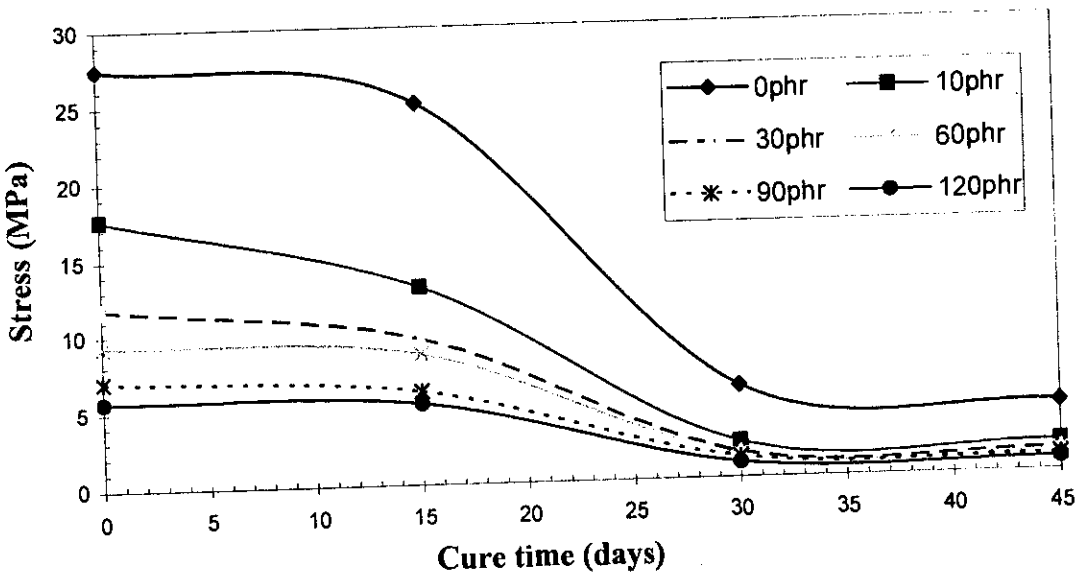

Fig(4.41). Effect of cure time on the tensile stress of RFCs at different ferrite loading

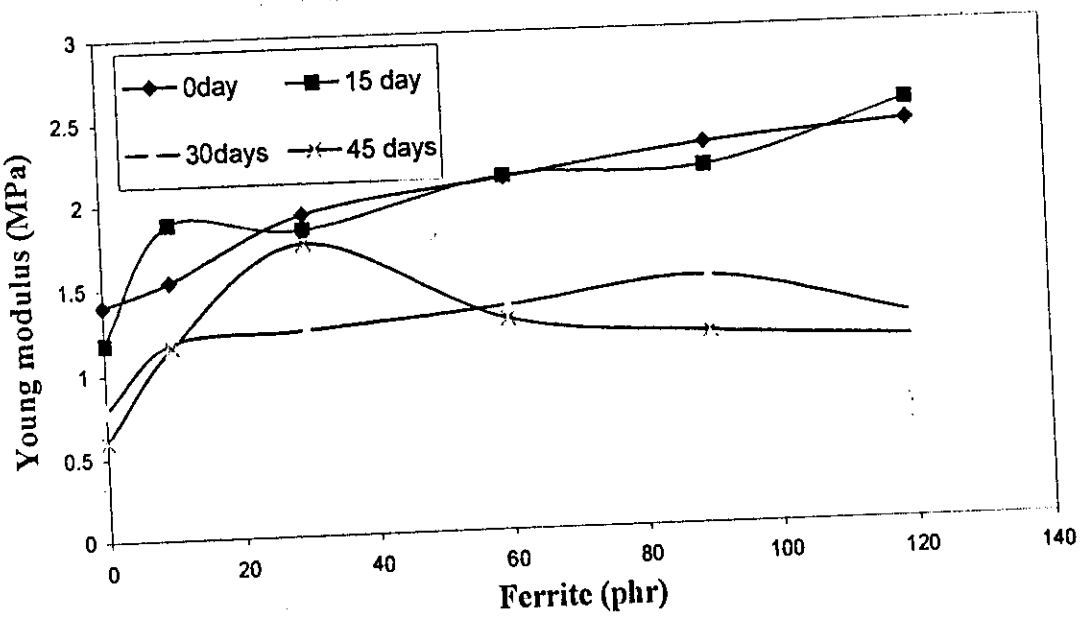

Fig (4.42) *Variation of Young modulus with ferrite loading at different aging time for RFCs*

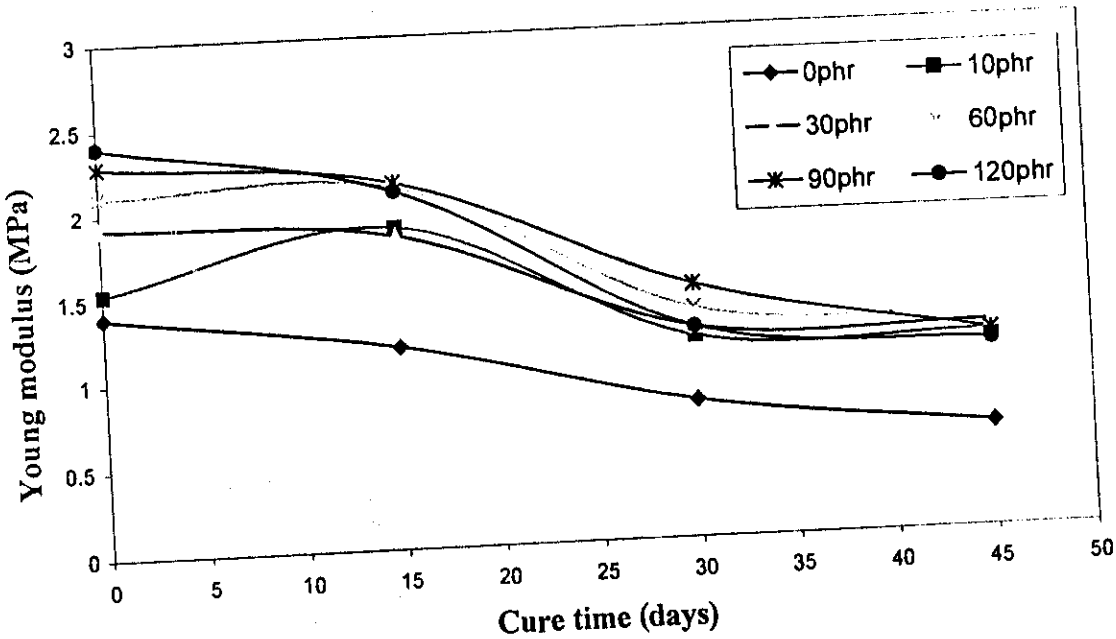

Fig (4.43) *Variation of Young modulus with aging time at different ferrite loading for RFCs*

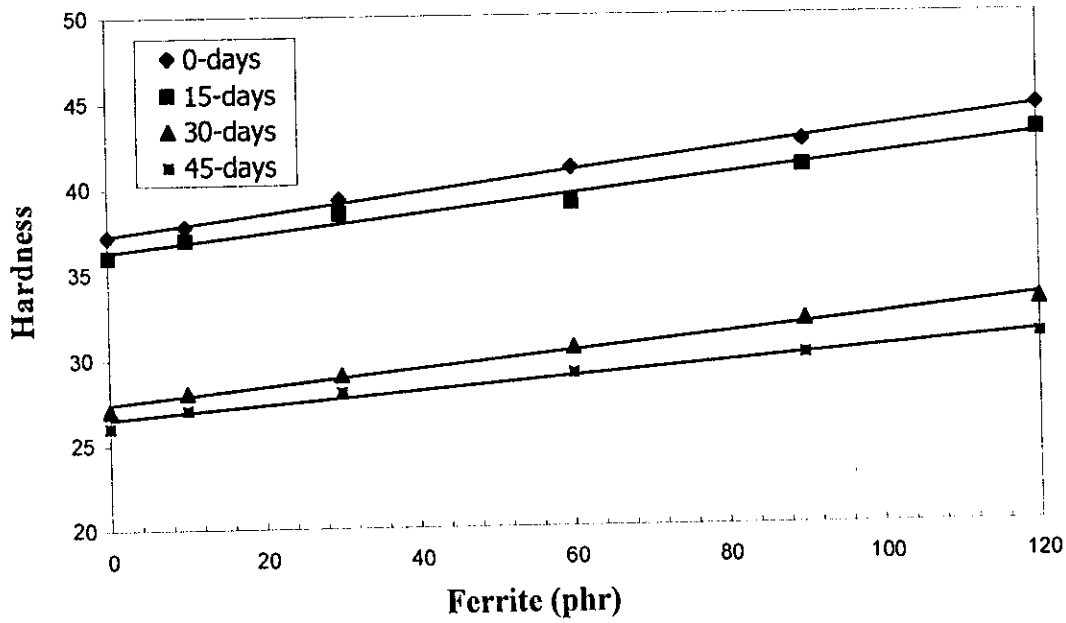

Fig (4.44) *Effect of ferrite loading on the RFCs hardness at different aging time*

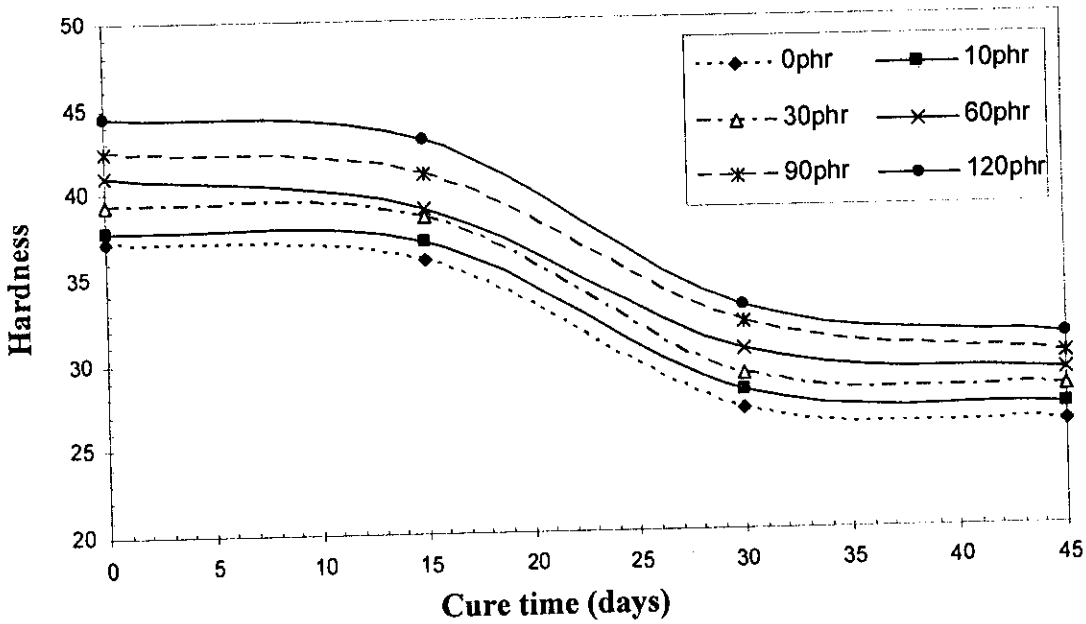

Fig (4.45) *Effect of aging time on the RFCs hardness at different ferrite loading*

An attempt was done to clarify the change in the mechanical characteristics, stress-strain, young's modulus, and shore hardness with increasing aging time for the present composites, using gelation technique [86].

The aged RFCs sample was heat treated in benzene, for 24 hours at the boiling point 80 °C . The samples swelled due to the penetration of solvent in the vulcanized rubber matrix. The losses percent in composite weight corresponding to the extracted linear portion of the rubber composite, and or the degradated chains at different aging times for the present samples are illustrated in figure (4.46). The results demonstrated that, thermal degradation occurred in rubber matrix due to the aging of RFCs composites up to 15 days, which appears as a dissolved of rubber matrix in the solvent leading to losses in composite weight. The weight losses increase after 15 days reaching asymptotic values beyond 30 days aging at 70 °C.

From the above study we can easily conclude that, the reduction in the mechanical properties with increasing barium ferrite loading and aging time may be due to the following reasons;

I- The poor interaction between the ferrite particles and the rubber matrix, which increase by increasing the ferrite fraction inside matrix, reduces both the stress and the elongation at break with increasing filler content. The weaker filler-rubber interaction would decrease the effectiveness of the stress transferred from the rubber matrix and consequently reduce the work required to deform the composites. Also the reduction in strength with increasing filler content suggests that the filler particles tend to debond from the matrix upon loading, and as a result of the decrease of the volume fraction [45]. Since

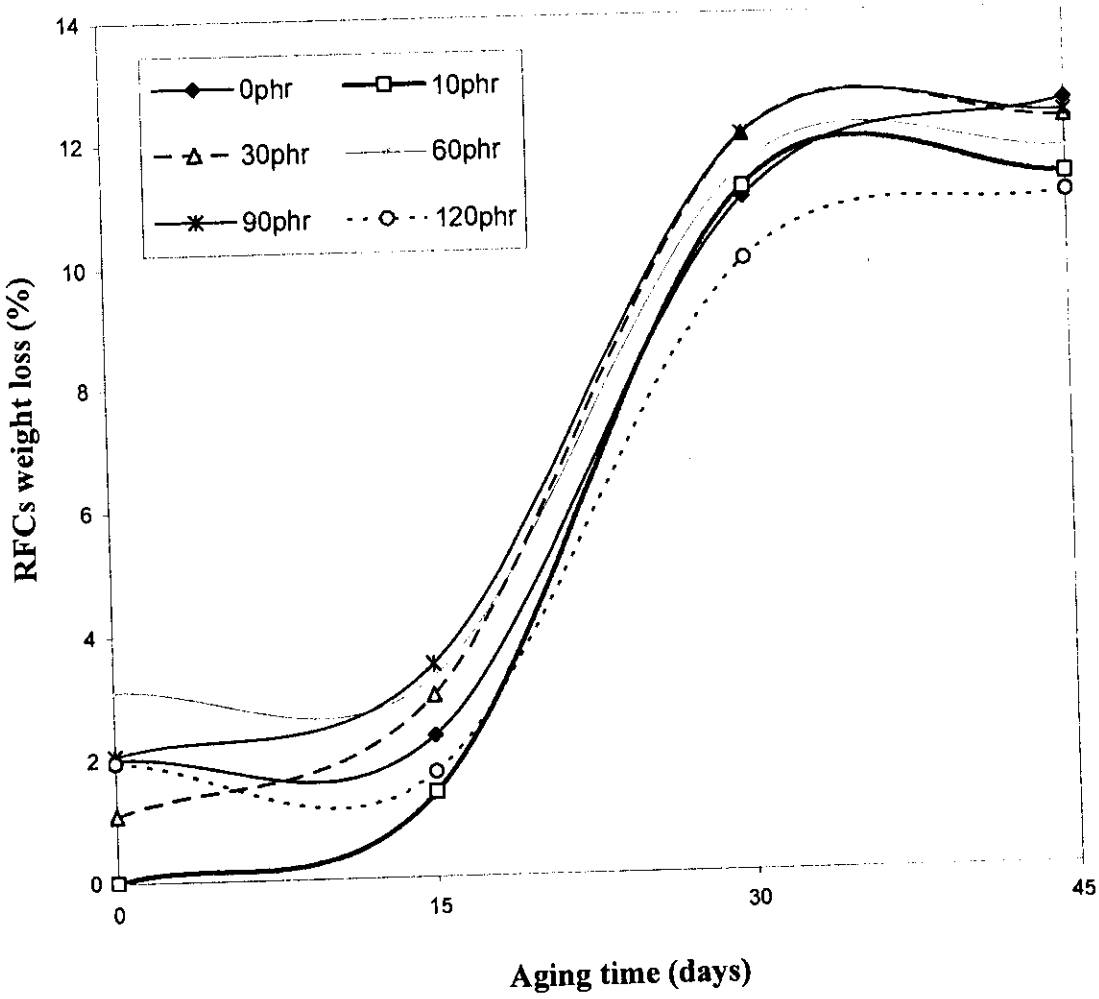

Fig (4.46) *Relative weight loss of RFCs versus aging time at different ferrite loading*

barium ferrite filler's particles are considerably large have irregular shape and smooth surfaces and untreated surfaces figure (4.23), thus the reduction in stress and strain are more drastically at low ferrite loading comparing with the spherical or small particles [53,87]. The little decrease with further addition of the filler, because, as mentioned before the coercive force starts to decrease by increasing the ferrite fraction in rubber matrix as a result of reducing the interspacing distance between ferrite particles , figure (4.32). In the other words, the increase of the particle interaction , as the interseparation distance decreases at high ferrite load, results in the rigidity of the composite matrix.

II- The degradation of rubber matrix with increasing aging time is also expected with long time of elongation. The properties of polymeric materials are dependent to a great extend on the length of their chains (i.e. on their molecular masses). By the thermal aging some of the weak vulcanized rubber bonds will split leading to a new substance with properties differing from those of the initial substance, which increase by increasing aging time.

4.3.3 Dynamic properties:

Figure (4.47) shows the change in the real ($\varepsilon^{\prime}$) and imaginary ($\varepsilon^{\prime\prime}$) part of storage modulus against the ferrite filler fraction. The modulii values were found to decrease after attaining maximum values and again increase at the higher filler loading. In contrast, the values of the damping factor δ and shore hardness tend to increase with increasing filler content as shown in figure (4.48).The attenuation in modulus is an evidence of the low interaction between filler particles themselves and filler-rubber matrix.

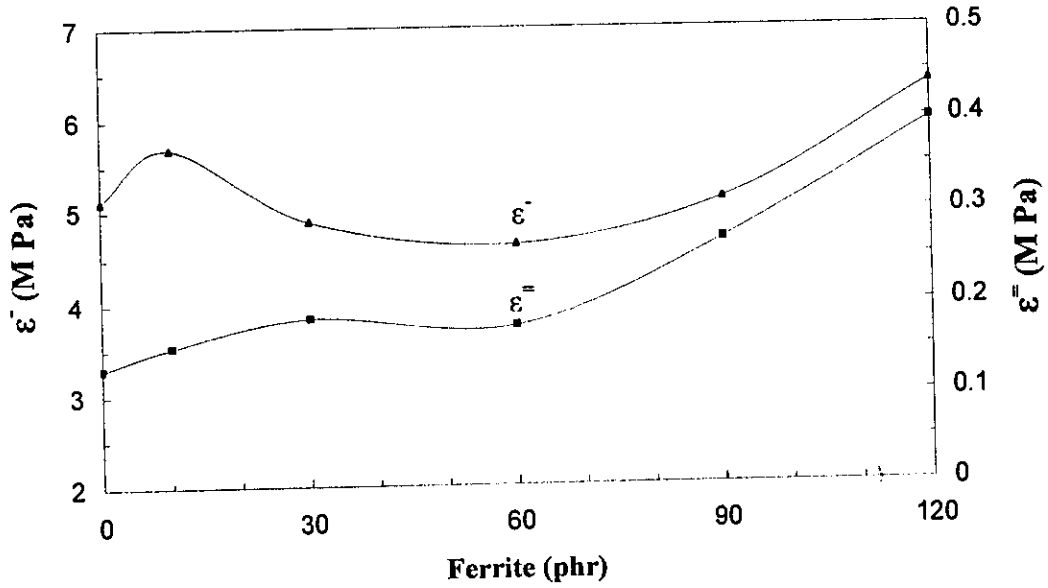

Fig (4.47) *The variation of storage modulus ε' and loss modulus ε'' with ferrite loading for RFCs*

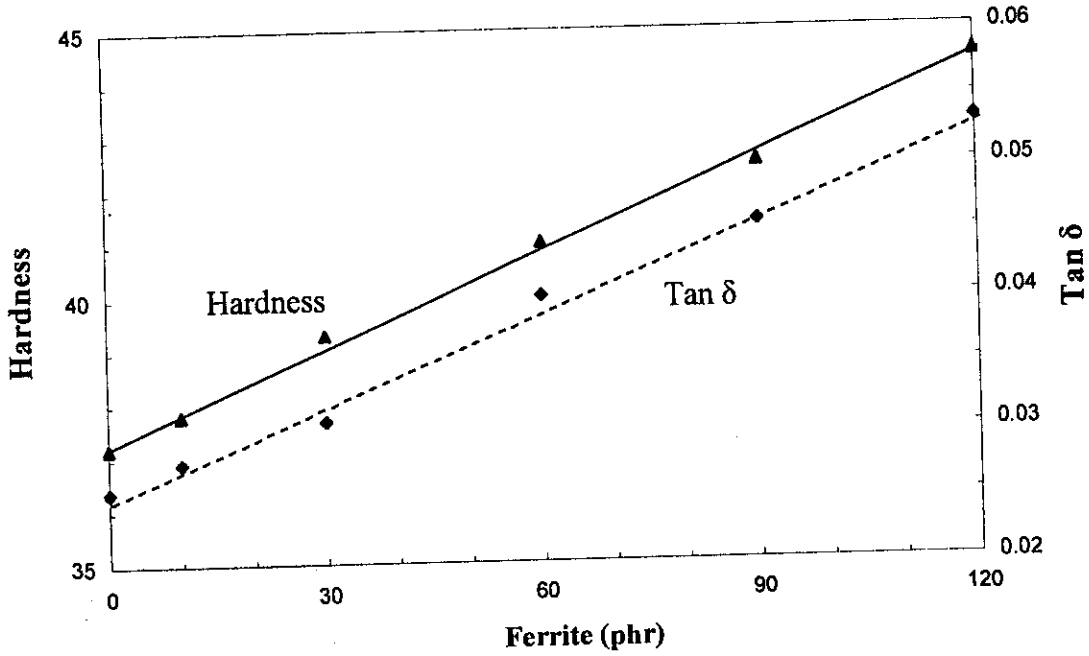

Fig (4.48) *The variation of RFCs hardness and Tan δ with ferrite loading*

There are numerous cases where the fillers increase the damping and consequently decrease the modulus [71]; (1) particle–particle friction where particles touch each other as in weak agglomerate, (2) particle–polymer friction where there is essentially no adhesion at the interface, and (3) excess damping in the polymer near the interface because of the induced thermal stress or changes in polymer confirmation or morphology. According to SEM micrograph figure (4.23) the particles in our RFCs are isolated from each other so that the attenuation in the modulus may be resulted from the particle-polymer friction. At low concentration of the filler there is a little friction and the modulus increases due to the incorporated rigid particles in the rubber matrix. By increasing the filler content the polymer- particle friction and their relative slapping will increase causing the increase of damping factor and decrease in modulus. It is also expected that due to the particle morphology, thermal energy released from the friction and slipping increase the damping in the polymer near the interface. By increasing the filler content furthermore the composite hardness reaches a high level and the particle-particle interaction increases as mentioned before due to the increase in surface interaction. Consequently the modulus starts to increase again with increasing filler content.

The composite resilience **R** was estimated according to the formula [34].

$$R = \exp(-\pi \tan \delta)$$

The variation of composite resilience with ferrite loading is indicated in figure (4.49). Clearly we see the resilience decreases with increasing ferrite.loading and the order of change is parallel to that of the modulus. The recorded values of resilience are considerably high comparing with the others work. It is a function

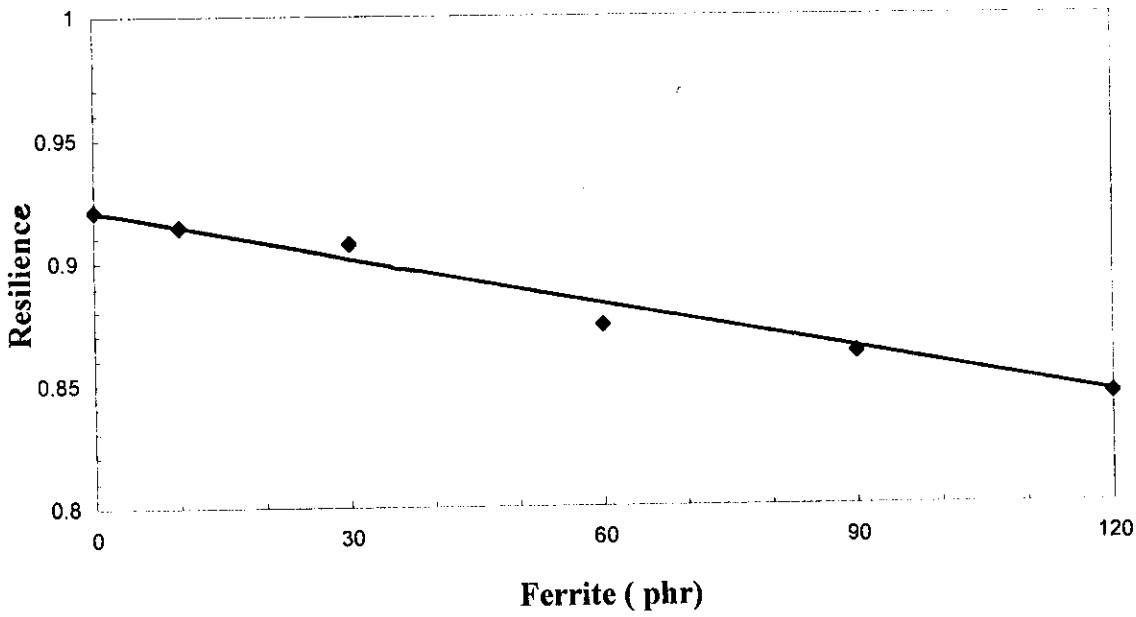

Fig (4.49) *Variation of RFCs Resilience with ferrite loading*

of the sulfur content and the type of the accelerator (high tensile accelerators) [34,88].

In general the increase of filler loading in natural rubber results in reduction of tensile strength , elongation at break and resilience , whereas it increases both of the tensile modulii and the hardness. Because of the increase of the filler loading leads to weakness the interface between filler and rubber matrix. The weaker filler-rubber interaction would decrease the effectiveness of the stress transferred from the rubber matrix and consequently reduces the work required to deform the composites [89].

4.4 Verification of the results

The final characteristics of our rubber-ferrite composites are listed in table (4.5) . At maximum ferrite loading 120 phr , the present RFCs recorded H_c = 5.3 KOe, M_s = 37.12 emu/g , density = 2.21 g/cm^3, $(BH)_{max}$= 1.17 MGOe , stress at break = 5.3 MPa, elongation at break = 48 %, storage modulus = 6.3 MPa, hardness= 44.5 , and resilience = 0.84 . The recorded values are considerably high for the magnetic results and they are reasonable for mechanical properties comparing to the other commercial products.

The data listed below are companies' catalogs, 2003, for high energy flexible magnets. Fillers are strontium and barium ferrites [90-93];

Mass fraction (%)	----	9.09	23.07	37.5	47.36	54.54	100
Load (phr)	----	10	30	60	90	120	----
H_c (KOe)	5.36	5.360	5.36	5.35	5.31	5.3	5.2
M_s (emu/gm)	----	6.25	15.28	24.26	31.76	37.12	68
Density (gm/Cm^3)	1.35	1.43	1.59	1.79	1.98	2.21	6.19
$(BH)_{max}$ (MGOe)	----	0.12	0.26	0.63	0.93	1.17	7.23
Stress at break (Mpa)	27.4	17.6	11.76	9.3	7.1	5.3	
Elongation at break (%)	11.6	8	5.5	5.5	5.33	48	----
ε (Mpa)	5.1	5.7	4.88	4.63	5.11	6.3	----
Hardness	37.2	37.8	39.3	41	42.5	44.5	----
Resilience	0.92	0.914	0.9	0.874	0.862	0.84	----

Table (4.5) Magnetic *and mechanical characteristics of the present barium ferrite-rubber composites*

THE MAGNET SOURCE™

TYPICAL MAGNETIC PROPERTIES OF HIGH ENERGY FLEXIBLE MAGNETS

High Energy Flexible Material	Density		Maximum Energy Product	Residual Induction Br	Coercive Force Hc	Intrinsic Coercive Force Hci
(BH Max)	lbs/in^3	g/cm^3	MGO	Gauss	Oersted	Oersted
1.1	0.128	3.542	1.10	2200	1900	2400
1.2	0.128	3.542	1.20	2300	1950	2400
1.3	0.128	3.542	1.30	2350	2000	2900
1.4	0.128	3.542	1.40	2450	2100	2900

Flexible Magnet Properties								
material	Br		Hcb		Hcj		BHmax	
	mT	Gs	KA/m	Oe	KA/m	Oe	KJ/m3	MGOe
XY-7	170	1700	96	1200	143	1800	5.6	0.7
XY-8	190	1900	107	1444	152	1900	6.4	0.8
XY-10	200	2000	120	1500	160	2000	8.0	1.0
XY-11	230	2300	160	2000	199	2500	10	1.25
XY-13	245	2450	160	2000	191	2400	11.2	1.4
XY-15	260	2600	160	2000	178	2200	12	1.5

NOTE: 1mT=10Gs 1KA/m=4лOe 1KJ/m3=4л×10MGOe

ARNOLD
THE MAGNETIC PRODUCTS GROUP OF SPS TECHNOLOGIES

Magnetic Properties

Property	CGS	SI
Br (Residual Induction)	2,730 G	273 mT
Hc (Coercive Force)	2,390 kOe	189 kA/m
Hci (Intrinsic Coercivity)	3,040 Oe	240 kA/m
BHmax (Maximum Energy Product)	1.80 MGOe	14.3 kJ/m^3
Reversible Temperature Coefficient of Induction, 20-100°C	-0.10% per °F	-0.18% per °C
Reversible Temperature Coefficient of Coercivity, 20-100°C	0.15% per °F	0.27% per °C
Required Magnetizing Force	10,000 kOe	790 kA/m

Mechanical Properties

Property	CGS	SI
Tensile Strength	Approx. 900 psi	Approx. 6.2 MPa
Elongation at Yield	Approx. 5 %	Approx. 5 %
Elongation at break	Approx. 5 %	Approx. 5 %
Density	0.134 lb/cu in.	3.72 g/cc
Hardness	65 Shore D	65 Shore D
Maximum Recommended Operating Temperature	176 °F	80°C

[92]

MMC Magnetic Materials & Components

Grade	Max. Energy Product		Remanence		Coercive Force				Work Temp.	Tensile Strength
	(BH)max		Br		Hc		Hcl		Tw	kg/cm^2
	MGOe	kJ/m^3	kG	mT	kOe	kA/m	kOe	kA/m	°C	
FLX07	0.8-1.0	6.5-8.1	1.9-2.0	190-200	1.7-1.9	135-151	1.9-2.0	151-159	40to 85	50-70
FLX11	1.4-1.5	11.0-11.8	2.4-2.5	240-250	2.0-2.1	159-167	2.6-2.9	206-230	40to 85	35-75
FLX11N	1.4-1.5	11.0-11.8	2.4-2.5	240-250	2.1-2.2	167-174	3.3-3.8	262-302	40to 85	20-30
FLX13	1.5-1.6	11.8-12.6	2.5-2.6	250-260	2.1-2.2	167-174	2.6-2.9	206-230	40to 85	50-70
FLX13N	1.5-1.6	11.8-12.6	2.5-2.6	250-260	2.1-2.2	167-174	3.3-3.8	262-302	40to 85	20-30

Heat Expansion Modulus (°C)	28 X 10^{-5}
Hardness (Shore A)	90 - 100
Density	3.6 - 3.7 g/cm^3

[93]

6- Both of elongation at break and stress decrease with increasing the ferrite powder in the rubber matrix, they are highly influenced by size shape and volume fraction of the particles. At the same time coercivity and saturation magnetization improved.

7- The dynamic properties are strongly dependent on the particles and particle-matrix characteristics than the magnetic and the mechanical properties. The present samples recorded, density= 2.2 g/cm^3 , BH_{max}= 1.18 MGOe, and resilience = .844 at 120 phr of ferrite.